NASA Contractor Report 195482

In-Phase Thermomechanical Fatigue Mechanisms in an Unidirectional SCS-6/Ti 15-3 MMC

Golam M. Newaz
Battelle Memorial Institute
Columbus, Ohio

and

Bhaskar S. Majumdar
Universal Energy Systems
Dayton, Ohio

June 1995

Prepared for
Lewis Research Center
Under Contract NAS3–26822

National Aeronautics and
Space Administration

IN-PHASE THERMOMECHANICAL FATIGUE MECHANISMS IN AN UNIDIRECTIONAL SCS-6/Ti 15-3 MMC

FINAL REPORT

to

NASA LEWIS RESEARCH CENTER
HITEMP OFFICE

Contract No. NAS3 -- 26822

Program Monitor: Dr. Bradley A. Lerch

Golam M. Newaz
Battelle Memorial Institute
505 King Avenue
Columbus, Ohio 43201

and

Bhaskar S. Majumdar
Universal Energy Systems
4401 Dayton-Xenia Rd.
Dayton, Ohio 45432

ABSTRACT

The objective of this investigation was to identify the inelastic deformation and damage mechanisms under in-phase (IP) thermomechanical fatigue (TMF) in a unidirectional SCS-6/Ti 15-3 metal matrix composite (MMC). Load-controlled IP TMF tests were conducted at 300-538 °C at various stress ranges in high-purity argon. A major emphasis of this work was to identify damage mechanism well before final fracture of specimens, rather than to generate life diagrams, to aid development of a realistic deformation/damage and life model.

The experiments showed that the principal damage mechanism under IP TMF was distributed cracking of fibers without any matrix cracks. It also was found that distributed fiber cracking was progressive on a cycle basis, that the density of cracks at a given cycle number increased with the applied stress level, and that a threshold applied stress, whereby fiber cracking can be avoided altogether, may not exist. The implication is that fiber cracking has to be considered in any IP TMF loading situation. At a number of locations in a given specimen, fiber cracks were found to be nearly coplanar over a few (3-4) adjacent fibers, and in few specimens the coplanarity extended over a significant fraction of specimen width in a given ply, i.e., they were "banded". Specimens with significant banding had high ratchetting rates and short TMF lives. Such banding is typically not observed under creep conditions, and suggest local stress concentration under IP TMF conditions. Comparison of ratchetting and fiber damage behavior under IP TMF conditions with companion creep and isothermal fatigue tests suggest that the thermal excursions in a given cycle contribute significantly to fiber damage accumulation. The fiber crack density was observed to be much less for a 16 minute cycle that for a 2-minute cycle, and possible reasons are suggested. Residual strength tests at room temperature following IP TMF cycles, and examination of fiber fracture density before and after residual strength test at RT, indicated little if any degradation of fiber strength due to the IP TMF cycles in the inert environment. Ratchetting responses were compared with the given ply, i.e., they were "banded". Specimens with significant banding had high ratchetting rates and short TMF lives. Such banding is typically not observed under creep conditions, and suggest local stress concentration under IP TMF conditions. Comparison of ratchetting and fiber damage behavior under IP TMF condition with companion creep and isothermal fatigue tests suggest that the thermal excursions in a given cycle contribute significantly to fiber damage accumulation. The fiber crack density was observed to be much less for a 16 minute cycle than for a 2-minute cycle, and possible reasons are suggested. Residual strength tests at room temperature following IP TMF cycles, and

examination of fiber fracture density before and after residual strength test at RT, indicated little if any degradation of fiber strength due to the IP TMF cycles in the inert environment. Ratchetting responses were compared with the predictions of a creep model that accounted for periodic fiber fracture. While agreement was reasonable for isothermal conditions, comparisons with IP data suggested that allowance must be made either for characteristic fiber strength degradation or a stress concentration effect; the former is unlikely based on the experimental results.

TABLE OF CONTENTS

LIST OF TABLES

LIST OF FIGURES

LIST OF FIGURES (continued)

LIST OF FIGURES (continued)

IN-PHASE THERMOMECHANICAL FATIGUE MECHANISMS IN AN UNIDIRECTIONAL SCS-6/Ti 15-3 MMC

INTRODUCTION

In engine applications, high temperature MMCs such as titanium-based silicon carbide fiber reinforced composites and their structural components will experience repeated combined thermal and mechanical loading. Thermomechanical fatigue (TMF) loading is thus a definite possibility for many of these components. The thermal part of the loading in a combined thermal and mechanical loading environment may result in a greater degree of viscoplasticity for the matrix. In addition, damage entities such as fiber cracks may lead to complex interaction of the constituents affecting the overall response of the MMC. Designing with MMCs, therefore, calls for a better understanding of the deformation and damage accumulation mechanisms in these materials under TMF loading conditions. In addition, lifetime assessment is an important need for structures made from MMCs as life prediction approaches are not well established for this type of new material system and their structures.

Previously, we had investigated [1-11] the inelastic deformation mechanisms such as plasticity and damage in SCS-6/Ti 15-3 MMC under monotonic tension, compression, creep and isothermal fatigue (IF) loadings. The focus of all of these studies was to evaluate the plasticity and damage mechanisms in unidirectional MMCs and their effect on MMC response. Furthermore, the effects of plasticity and damage and their relative roles on the inelastic deformation response of MMCs were clarified. For example, our previous investigation of IF [11] showed that strain ratchetting (due to stress relaxation effects in the matrix) occurred at elevated temperatures [11], that fiber matrix debonding and fiber fracture were the characteristic damage mechanisms in Regime I (high applied stress range), and that matrix cracking was the predominant damage mode in Regime II (intermediate applied stress range). These regimes are illustrated in Figure 1.

Our previous efforts were to develop a comprehensive understanding of the damage mechanisms rather than to obtain fatigue S-N curves for isothermal fatigue loading, and this approach is continued in the current TMF investigation. The overall objective of this study was to determine the inelastic deformation mechanisms that influence the response of the MMC under IP TMF. Additionally, we have provided a framework for a mechanism-based life model for distributed fiber cracks - a characteristic damage mechanism observed under IP TMF [12-19].

With respect to life prediction, mechanism-based models are not fully developed. Rather, several phenomenological TMF models have been suggested by researchers [13,18]. In one study, a linear life fraction model (LLFM) was shown to have promise for TMF life prediction [13]. In another study, it was suggested that TMF lives for both in-phase (IP) and out-of-phase (OP) loadings depend on a single correlating parameter, namely, the fiber stress in the unidirectional ply [18]. However, in both cases, the intrinsic damage effects at the microstructural level are ignored and evolution of damage is not considered. Because of the complexity of the deformation response under TMF loading as they pertain to the matrix, fiber and fiber-matrix interface, analytical formulations describing the role of damage and viscoplasticity and their effects on load sharing between the fiber and the matrix are missing. It is not known, for example, if there is an applied stress level below which there would not exist any fiber cracks, how the fiber damage and matrix viscoplasticity combine to influence ratchetting rates and final failure of the MMC, whether there exist fiber cracking characteristics/kinetics that can be used adequately predict the ratchetting response under IP TMF, etc.. In order to facilitate the development of a mechanism-based model, we examined the various mechanisms and the failure modes as they evolved as a function of IP TMF cycles.

A large number of TMF characterization studies have been conducted by researchers in the past few years emphasizing testing, performance and prediction of life [12-22]. Many of the studies have focused on the relative life differences when the MMC is subjected to thermal fatigue, IF, IP and OP TMF (Figures 2 and 3). The TMF studies have shown that in-phase TMF loading for unidirectional composites results in distributed fiber fracture. Analytical modeling was undertaken as well [23]. However, an explanation is lacking as to the real cause of the initiation and accumulation of the distributed fiber cracks. Furthermore, implications on the TMF life of the MMC due to the presence of these cracks have not been addressed.

A review of these previous investigations points out several important issues:

- Is distributed fiber cracking an inherent mechanism during IP TMF, and is it progressive on a cycle to cycle basis? If so, is there a growth law relating the density of fiber cracks to either the number of cycles at a given stress level or to the magnitude of accumulated MMC strain?

- Is there an applied threshold stress for the MMC below which fiber fracture can be avoided under IP TMF? A threshold level would be useful in design.

- What is the role of the thermal cycle component in an IP TMF cycle?

- Is there fiber strength degradation during IP TMF?

- What is the effect of IP TMF cycles on residual strength at RT? The later data are often important in design considerations.

- What is the role of cycle time on IP TMF life? Possible effects include non-uniform temperature distribution in the constituents at high frequencies, and the influence of matrix stress-relaxation on TMF damage accumulation and life.

- How does IP TMF damage differ from those under creep conditions?

- What is the effect of IP TMF on interface strength?

- What is the explanation for the absence of any compliance change in IP TMF even in the presence of high fiber crack density ?

- Finally, based on the mechanisms, what is an appropriate framework for an IP TMF life model?

To address these issues, we conducted a selected set of experiments. *In doing so, we emphasized mechanisms, and concentrated on events that occur well before MMC fracture, since under probable statistical circumstances neighboring fiber fractures could produce highly localized damage and premature failure.* The rationale was that such understanding is necessary for developing any realistic life prediction methodology. *Developing a database for S-N curves was not the objective of the program..* Some initial results and discussions of the work are available in references [24-26], with [24,26] providing TMF data on a 15 volume percent MMC, and [25] providing additional data on fiber strength statistics and the characteristics of "banded" fiber fracture.

EXPERIMENTS

Material and Specimens

All in-phase TMF experiments were performed on 8-ply 0° SCS6/Ti 15-3 MMCs with 41 volume percent fibers (MMC-41). This material was consolidated by Textron Specialty Metals using a foil-fiber-foil process, and all of these panels utilized Mo-weaves to hold the fibers in place during consolidation. To assess the effects of the Mo-weaves, 4-ply panels were produced by the arc-spray method at NASA-LeRC. These plates had a fiber volume fraction of 30% (MMC-30) and did not contain Mo-weaves.

All tests were performed on the as-received materials, without any further heat treatment. In this condition, the microstructure is relatively clean, which allows easier understanding of the effects of TMF deformation on the dislocation structure in the MMC, and how fatigue cracks nucleate. Note that Ti-15-3 (Ti-15V-3Cr-3Al-3Sn alloy, all weight percent) is a metastable beta Ti-alloy with a body centered cubic (bcc) crystal structure, and in reference [1,2] we had shown that it contains a very fine omega (hexagonal close packed, hcp) phase which gives the material a planar slip character at room temperature. At temperatures above 300 C, acicular alpha-phase (hcp) particles are known to precipitate in the microstructure with a fixed orientation relationship with respect to the parent bcc phase. Heat treatments at temperatures between 400 C and 550 C produce finer precipitates, and they increase the modulus by about 10 percent. In most of the past fatigue studies on the SCS6/Ti 15-3 system, the MMCs were subjected to a 700 C/24 hour heat treatment with the aim of stabilizing the microstructure; such a heat treatment does not alter the modulus of the matrix alloy by any significant amount compared with the as-received material. However, this type of heat treatment cannot prevent the formation of new finer alpha phases when the specimen is tested or held at intermediate temperatures; i.e., microstructural evolution is an integral part of the Ti 15-3 system at elevated temperatures.

The specimen geometry used for in-phase TMF testing is shown in Figure 4. Evolution of this design is described in Ref. 11.

Experimental Conditions

Experiments were performed in the load control mode on a servohydraulic test system equipped with water-cooled friction grips. All tests were performed at an R-ratio of 0.1. The temperature cycle was 300-538 C for a 120 sec cycle. A typical stress-temperature

history from an IP TMF test is illustrated in Figure 5, showing that the temperatures and stresses were in-phase and followed a linear ramp profile; time differences at the extremum points ranged between 1 and 4 seconds.

The TMF tests were performed using induction heating in a stainless steel chamber which was initially evacuated to 10^{-4} torr of vacuum, then backfilled with high-purity gettered argon. Some tests were performed with an initial evacuation to 10^{-6} torr, but test results did not show any systematic variation in ratchetting or life between pre-evacuation at 10^{-4} and 10^{-6} torr vacuum. An argon flow rate of 3 liters/minute was maintained during the tests. The inert atmosphere was used to keep oxidation to a minimum, so as to interpret TMF response in terms of the MMC's inherent characteristics rather than the environment. Specimen strains (over a 12.5 mm gage length) were monitored at the specimen edges using an extensometer with ceramic arms, and the stress-strain data were recorded digitally at different fractions of life.

TMF tests were followed by detailed microstructural characterization, to identify damage and failure mechanisms. Interrupted TMF tests were conducted to monitor damage evolution and these specimens were metallurgically examined. The fracture surfaces were examined using optical and scanning electron microscopes.

Design of Experiments

To provide insight and background on the results that are presented later, a brief description of the different types of experiments are listed here, including rationale for their selection:

(i) Obtain initial assessment of life and strain ratchetting under IP TMF loading, and compare with data from IF tests performed at 538 C at both 1 Hz (baseline) frequency as well as at approximately 0.01 Hz (actually 0.00833 Hz, same frequency as the TMF tests). Experiments were conducted at maximum stresses of 1114 MPa, 1000 MPa, and 850 MPa. Although there was significant scatter in TMF life and the ratchetting response, a characteristic unifying feature of all specimens was a high density of fiber cracks. A decision was made to understand the fiber fracture issue, and this dictated design of subsequent experiments.

(ii) Interrupt tests at various fractions of life at a given stress level, followed by destructive metallographic evaluation of fiber damage. These experiments would provide data on progressive fiber fracture kinetics. A 114-1114 MPa/ 300-538 C in-phase cycle

was selected. Initial tests showed one failure at 96 cycles, and no failure even after 7516 cycles. Interruption was designed for 3, 30, and 60 cycles. As will be discussed later, the probabilistic nature of cracking offset this simplistic method of evaluating fiber damage evolution.

(iii) Perform tests at different stress ranges, but unload after approximately 300 cycles, followed by metallographic evaluation of fiber damage. The objective was to determine if a stress range existed below which there was no fiber fracture. Viscoplastic analyses indicated that in the absence of fiber fracture, most of the ratchetting and load dumping to fibers would be over well before 300 cycles, so that 300 cycles could be a good stopping point for evaluating any fiber damage. Stress ranges as low as 30-300 MPa were utilized.

(iv) Determine the strength of fibers removed from the as-received specimen by etching away the matrix. This data would provide the statistical strength distribution of fibers in the panel, to help explain if a possibly weak fiber population existed in the panel, which could explain why fiber fractures were observed in specimens that were subjected to very low stresses (30-300 MPa). Single fibers from the MMC-41 were removed from an untested specimen and the fibers were tested at NASA-Lewis Research Center. The matrix was etched away using a solution of 85 percent water, 10 percent HF and 5 percent HNO_3. The fibers were rinsed in water and dried in air. Tensile tests were conducted at 0.13 mm/min cross-head speed. Forty fibers were tested.

(v) Evaluate whether TMF as well as thermal cycles (without loads) damage the SCS6 fibers, which have a rather complex structure consisting of different grades of carbon and SiC with their own thermal expansion coefficients and elastic modulus. Examination of IP specimens indicated that fibers were failing at apparent average stresses well below those determined from the individual fiber strength tests. The approach consisted of the following: after 300 IP TMF cycles at 30-300 MPa, metallographically polish the specimen to the first fiber layer and assess fiber break density. Then load the specimen at RT to 0.8% strain, sufficient to raise the average fiber stresses to about 3000 MPa. Then polish the other face of the specimen to the fiber level to assess if the crack density increased. The rationale was that any incipient fiber damage due to TMF, that did not show up as a fiber break following cycling at 300 MPa, would most likely lead to distributed fiber breakage at the high stress at RT, and hence a higher fiber crack density. On the other hand, if fiber degradation was small or negligible, then the crack density would be the same, both before and after the tension loading at RT.

(vi) Evaluate whether the reasonably rapid TMF cycles (2 minute duration) introduce significant fiber stress elevation through either (a) non-uniform temperature profile in the constituents (for example, fibers could be at a lower temperature than the matrix, thereby causing fibers to fail at low apparent fiber stresses), or (b) through possible retention of reasonable fiber-matrix clamping stress, and hence higher friction stress at broken fiber regions (compared with a creep case), resulting in stress concentration in fibers adjacent to isolated fiber breaks at random weak locations. This issue was addressed by testing companion samples at 700 MPa with cycle durations of 16 minutes and 2 minutes.

(vii) Evaluate the effect of TMF cycling on interface strengths, to understand how a broken fiber influenced stress elevation in neighboring fibers. The interface strength values could also be used to obtain more accurate estimate of crack spacings in a particular fiber; crack spacings appeared to be well below values calculated by a shear lag analysis.

(viii) Determine the residual strength of an IP cycled specimen at RT, to evaluate the extent by which fiber failures influence tensile strength.

(ix) Confirm whether fiber fracture also occur in creep at reasonably low applied loads, such that strain saturation is reached. A stress of 700 MPa was selected, and IP TMF tests had indicated significant fiber fractures at this stress level.

(x) Perform thermal cycling at a constant load, to determine if the thermal cycling component contributes to fiber fracture; stresses of 165 MPa and 700 MPa were selected.

(xi) Evaluate whether intrinsic MMC defects play a significant role in the statistical nature of fiber fractures. In particular, Mo weaves appeared to influence locations of the initial fiber fractures, although at a later stage of life fiber cracks were observed far from the weaves. Therefore, a small panel of SCS6/Ti-15-3 MMC was fabricated at NASA Lewis using the powder cloth process, without incorporating any Mo weave. These specimens had only 30 volume percent fibers, and so stress levels were scaled according to the fiber volume percent. The experiments were designed to understand whether the progression mechanism of fiber damage was different with and without Mo weaves, or whether there was a matrix-microstructure independent fundamental fiber breakage mechanism that was operative under IP TMF, but which was possibly accelerated by matrix defects.

RESULTS

Mechanical Response

A summary table describing all the tests is presented in Table 1. The table is arranged by specimen number and represents the order of testing in an attempt to investigate the fiber cracking mechanism in a chronological manner. In general, the rationale for subsequent tests were determined based on the results of the previous series of tests. Given the high crack density of distributed fiber cracks for tests at higher stresses such as 1114 and 850 MPa (specimens F41-1 to F41-8 except F41-6 and F41-7 which were conducted to determine the early fiber crack development), the maximum stress was lowered to 700 MPa followed by 165 MPa and to 300 and 400 MPa to determine if fiber cracks occurred even at very low stresses (specimens F41-9 to F41-18). These series of tests can be categorized as lower stress tests. Specimens F41-19 to F41-24 series of tests can be categorized as confirmatory tests to help confirm our understanding of the fiber cracking mechanism from the previous series of tests. The last three tests (B1-1 to B-3) were with the MMC-30 specimens without the Mo-weave. Table 2 represents tests in Table 1 that are organized by maximum stress values, other important test data, and also provides information on damage state.

Figure 6 shows the monotonic response of MMC-41 and MMC-30 specimens. It is noted that MMC-30 has somewhat lower modulus (160 GPa), although strength (1600 MPa) and strain-to-failure (1.2%) are comparable to 35 volume fraction MMC [1]. The tensile strength of MMC-41 was about 1400 MPa. MMC-30 had a large amount of porosity due to incomplete consolidation which most likely lowered the modulus value.

A number of TMF tests were carried out at a maximum stress level of 1114 MPa which is roughly equal to 80% of the ultimate tensile strength. The test data (Tables 1 and 2) indicate significant scatter in life at this stress level, with a failure at only 15 cycles and a run-out at 7516 cycles. TMF tests were carried out at a maximum stress level down to 300 MPa. A few tests were conducted at a very slow thermal cycling rate of 16 minute per cycle as opposed to the typical rate of 2 minutes per cycle. A number of tests were conducted (F41-12 and F41-13) with a constant load e.g. 165 MPa and 700 MPa, respectively, with thermal cycles between 300-538 C to explore if thermal cycling in the presence of a load was enough to initiate distributed fiber cracks. A creep test (F41-24) was conducted to better understand the nature of creep damage in the MMC in relation to IP TMF damage and also to better interpret the ratchetting response in IP TMF.

A TMF life plot is shown in Figure 7. In this plot, the arrows represent specimens that were tested and removed prior to failure to examine the evolution of damage. Isothermal fatigue data from the literature are also included in Figure 7 for comparison purposes. Note that at 1114 MPa maximum stress, one particular TMF test (F41-5) lasted longer than two IF tests at 538 C (an IF life of 2296 cycles at 1 Hz, and an IF life of 3895 cycles at 0.00833 Hz [24,25]). However, while only fiber damage was observed for the IP specimens, the IF specimens had matrix cracks, as well as isolated fiber cracks. In fact, small regions of matrix crack growth were observed on the fracture surfaces of the IF specimens, and may explain why IF life was lower than the IP specimen (although this particular IP test appears more of an exception, given the short failure lives for the other specimens at the same stress level). The absence of matrix cracks in the IP specimen can be explained by the fact that the matrix strain/stress range, which governs matrix crack growth, is lower under IP conditions than under IF conditions. Simple thermal stress calculations show that the temperature changes in a cycle reduce the matrix stress range by about 80 MPa (between 300 and 538 C), and for an effective matrix modulus of about 60 GPa (considering viscoplastic deformation) this would imply that the matrix strain range is reduced by approximately 0.13%. Using a strain range versus life plot, as in references [24,25], this would imply a matrix dominated life of about 20,000 cycles; i.e., in an IP test at 1114 MPa, a matrix dominated failure would kick in at lives approaching 20,000 cycles (if fiber-dominated failure did not occur earlier), whereas it can occur as early as approximately 2000 cycles in an IF test at the same maximum stress level. Nevertheless, considering that four IP samples at a maximum stress of 1114 MPa failed in less than 100 cycles, we can only conclude at this stage that there is a high probability of significantly shorter life under IP condition compared with IF condition at 1114 MPa maximum stress level. It will be shown later that specimen F41-5 with a run-out 7516 cycles had a very uniform fiber crack distribution, which may explain why ratchetting stabilized for this specimen and did not lead to early specimen failure.

Figure 7 also includes data on a 15 volume percent MMC (MMC-15), that was investigated in an initial part of this study [24,25]. On a maximum applied stress basis, the MMC-41 clearly outperforms MMC-15, indicating the expected payoff from the higher volume percent MMC. On a strain range basis, however, the IF data of MMC-15 and MMC-41 were comparable at lives typically higher than 10,000 cycles; i.e., in the matrix dominated regime. Under IP conditions, the life of MMC-15 was significantly shorter than MMC-41 even on a mechanical strain range basis [24,25]; i.e., the damaging influence of IP TMF appeared to be more severe for MMC-15 than MMC-41. While the ratchetting rates started out similar for companion IF (at 0.00833Hz) and IP samples at 50-506 MPa,

the ratchetting rate accelerated rapidly for the IP specimen and led to failure in 44 cycles, whereas the ratchetting rate decreased for the IF specimen, which was subsequently unloaded after 5630 cycles. It appears that the characteristic features responsible for early specimen failure under IP conditions for MMC-41 are also present for MMC-15. Additionally, significant elongation including necking occurred for MMC-15, since the matrix carries a substantial fraction of the load for such low volume fractions and can lead to unstable failure at much larger strains.

The TMF response, i.e., hysteresis loops from high, medium and low stress level tests are presented in Figures 8-10 with the corresponding minimum and maximum strain levels. In these plots, the mechanical strain range was obtained by subtracting the thermal strain from the total measured strain, using a thermal expansion coefficient of 5.8×10^{-6}/C for the 41 volume percent MMC; the expansion was computed from fiber and matrix properties using the concentric cylinder model. It is noted that in all cases, the strain range appears to be constant as a function of TMF cycles. The increase in maximum and minimum strains are manifestations of the ratchetting response of the MMC under in-phase TMF loading. Early strain rise in an IP TMF test with 1114 MPa as a maximum stress is presented in Figure 11. Figure 12 provides comparisons of the ratchetting response of the MMC-41 specimens under identical applied loads. In the plot, "F" and "DNF" denote failed and did-not-fail (unloaded), respectively. The ratchetting curves for the IP specimens show some scatter. While the maximum strain in the first cycle may be due to specimen-to-specimen variations and possible fiber cracking at first loading, the key information in Figure 12 is that the rate of ratchetting was faster for IP compared with IF specimens. Reduced recovery of the matrix strain on unloading under the IP condition (unloading at lower temperatures) compared with the IF condition may be responsible for a higher degree of ratchetting. This is believed to be further aided by fiber cracking, which appeared to be significantly enhanced under IP TMF conditions.

Several tests were run at considerably higher cycle times, e.g., 16 minutes compared with 2 minute cycles. As already indicated, one purpose of this test was to evaluate if non-uniform temperature distribution might play a role in enhancing fiber fracture, given that a 2 minute cycle time may be insufficient to provide temperature uniformity throughout the specimen. At the same time it is realized that for a given number of cycles, a longer cycle time would produce rapid creep deformation of the matrix, and hence possibly more fiber fracture. Comparisons of Figures 9 and 13 illustrate the expected trends, in that for the 2 minute cycle, ratchetting extended rather uniformly over many cycles. On the other hand, for the 16 minute cycle, ratchetting was rapid initially, but the rate decreased with cycle numbers. The total amount of ratchetting was actually less for

the 2 minute cycle (approx.0.14%) than for the 16 minute cycle (approx.0.22%). However, it will be shown later that the 2 minute cycle produced many fiber cracks, whereas the number of cracks for the 16 minute cycle was significantly less.

To investigate the influence of distributed fiber cracks on the residual strength of the MMC specimen, one test was done (F41-23) after the specimen was subjected to 300 IP TMF cycles at an 850 MPa maximum stress. Although, we recognize that statistical variability on strength is a reality, the single test was performed primarily to determine if there is a significant reduction in strength. The residual strength obtained was about 1300 MPa which is close to the ultimate tensile strength of 1400 MPa for the MMC-41 composite. Based on our tests at 700 MPa for 200 and 300 cycles, and the reasonable density of fiber cracks observed in such specimens, as well as investigation of a 850 MPa specimen which lasted 8161 cycles, we expected a reasonable distribution of fiber cracks in this specimen prior to the residual strength test. It appears that the residual strength is not significantly affected by distributed fiber cracks.

The primary intent of the research effort was to investigate the fiber cracking mechanism and to clarify a number of issues as discussed in the introduction. Accordingly, the majority of tests were interrupted before failure(Table 1). In most cases, we stopped the tests between 3 and 300 cycles to investigate the chronological evolution of damage, and including those data on lifetime plots do not provide any valuable information. They can be reviewed in Table 1 or Table 2. However, for the 1114 MPa to 850 MPa maximum stress, TMF data (F41-1, F41-2, F41-3, F41-5, F41-19 and F41-20) provide some useful information in that the variability in lifetime within the stress values of 850-1114 MPa is evident. Typically, 10,000 TMF cycles is considered a large number of cycles. Therefore, specimens such as F41-2 and F41-3 which did not fail close to 10,000 cycles may be considered as runouts.

Interface measurements at RT on an IP specimen cycled at 1000 MPa stress for 4751 cycles (sample did not fail), indicated a friction stress of approximately 80 MPa. This value is lower than approximately 120 MPa measured for the as-received material, and points to some degradation of the interface due to IP loading. However, the scatter in data for the IP specimen was much more than the virgin material, and may be related to the fact that many of the fibers were broken and debonded in the IP cycled MMC.

A creep test (sample F41-23) was performed at 700 MPa. The stress was selected since calculations showed that the stress was low enough to preclude fiber fracture, and hence lead to attainment of zero creep rate at long times. Also, IP TMF tests at the same stress level indicated significant fiber cracks and ratchetting.

Microstructure

SCS-6 fibers are brittle ceramic fibers and it is possible that fibers may crack during processing. Also, there exist questions regarding the polishing technique; i.e., whether fiber cracks occur during polishing. As a reference, we polished an entire untested specimen to verify that there were no pre-existing cracks, and that cracks were not introduced during polishing. Figure 14 is a micrograph of that specimen. No cracks were observed in this ply. Such polishing has been previously performed on other untested specimens, and they too have indicated none or at most a few (less than 10) pre-existing fiber cracks in an entire ply. On the other and, as will be shown later, fiber cracks were observed throughout the specimens of IP specimens, and they were observed previously in IF specimens cycled at high strain ranges (in Regime 1).

Specimen F41-5, which was unloaded after 7516 cycles, was metallurgically polished to its first layer of fibers. Optical microscopy revealed a high density of fiber cracks throughout the gage section (Figure 15). In order to establish that similar fiber cracks were present in other plies, the specimen was then further polished down to the third layer of fibers. Figure 16 shows distributed fiber cracks in this layer confirming that the fiber cracking phenomenon occurs throughout the bulk of the specimen and is not confined to surface layers only.

Figure 17 is a micrograph of specimen F41-7, which was unloaded after 30 IP cycles at a maximum stress of 1114 MPa. This specimen also shows significant fiber cracks at this low cycle number, and it is unlikely that the specimen would have survived many more cycles. Another interesting feature of Figure 17 is that the cracks appear to fall along a band, perpendicular to the loading direction. Such "banding", which for this specimen consumed a significant fraction of ply width, can be detrimental to the load carrying capability of the MMC. Specimens with very short lives had similar banding, but such severe banding did not occur in all specimens. More typical was the case where a limited number (about 3 to 4) of adjacent fibers had coplanar cracks (or something very close), which then got dissipated into more random crack locations in nearby fibers. Such coplanar cracks may be seen in most of the micrographs in this report, and their existence points to some form of stress concentration effect, along the lines analyzed by Hedgepeth and Van Dyke[28]. Banding or coplanarity has not been reported in past creep studies of MMCs. One possible reason is that the matrix stress, in particular the radial stress at the interface, is significantly relaxed under creep loading, so that when a fiber does fracture, debonding can occur readily. Consequently, a large volume of matrix can participate in transferring the excess load to the neighboring fibers; i.e., stress concentration would

accordingly be low at the crack plane on the nearby fiber. On the other hand, the thermal clamping of fibers during the unloading-cooling cycle in IP TMF may have associated with it some inelasticity, particularly at the broken fiber ends. This could possibly enhance the clamping and friction stresses during the reload cycle, resulting in higher stresses in the matrix near the crack plane, which in turn would load up the adjacent fiber only close to the crack plane; i.e., a stress concentration effect, resulting in faster propagation of fiber breaks. These arguments on stress concentration effects due to clamping, are qualitatively similar to the local versus global load sharing concepts advanced by He, Evans and Curtin [32]. According to their analyses, a high friction stress and low fiber strength can lead to failure of nearest neighbors rather than next nearest neighbors; i.e., local load sharing. If indeed clamping is an important reason for crack coplanarity, then a longer IP cycle time may actually be beneficial, since clamping stresses can get dissipated by the time full load is reached at maximum temperature. Note that these are at least a few explanations for crack coplanarity and banding, although other likely explanations may exist as well. More important, however, is the fact that crack coplanarity and banding do occur under IP TMF, and indicate that once some cracks initiate in fibers, they can spread more rapidly under IP TMF conditions than under other loading conditions. This can explain the significant damaging influences of IP loading on fiber fracture and low life, and is an issue that needs additional experimental and theoretical validation. From a life prediction viewpoint, it implies that in IP TMF, the main issue is the rate at which fiber damage progresses from one fiber to the next, rather than the occurrence of the first fiber crack.

An isothermally cycled (1114 MPa max. stress at 538 C) specimen (F41-4) was polished to evaluate its damage mechanisms and compare with the IP TMF mechanisms. It revealed surface matrix cracks and fiber fracture near the matrix crack plane (Figures 18 and 19). Isolated fiber cracks, without matrix cracks, were also observed at other locations of this specimen. These fiber cracks were more uniformly distributed, similar to the F41-5 IP TMF specimen. Besides the matrix cracks under IF conditions, another important distinction with IP TMF damage was that the fiber cracks were often associated with local debonding (Figure 19).

A high magnification photomicrograph of the fiber fracture surface in specimen F41-5 revealed several interesting fracture characteristics of the fibers. Careful observation showed that a large number of fibers failed due to crack initiation from the core and a similar number of fibers failed by crack initiation from near the fiber surface layers. There was no attempt to quantify the distribution of cracks from one type to the other type of fracture. Scanning electron photomicrographs of the two types of fiber fracture are shown in Figures 20 and 21.

There were two types of IP TMF fiber cracks: (a) single crack and (b) multiple "shatter" cracks as shown in Figures 22a and 22b. Whether they are surface or core initiated remains to be investigated. Studies conducted at Lawrence Livermore Research Laboratory revealed that SCS type fibers can fail by spiral cracks (Figure 23) which can manifest as a number of closely spaced crack systems at the fiber surface [27] resembling "shatter" cracks. Also, it was noted that in IP TMF, the fiber cracks were not typically associated with large debonds as in the case of IF (Figures 19 and 22) specimens.

The fiber cracks observed under IP TMF generally were very fine hairline cracks. Careful SEM evaluation showed that the crack surface displacements were submicron in size. We made fifteen measurements and the average COD was determined to be 0.3 μm. A typical separation of 0.3 μm is shown in Figure 24. The actual COD when the specimen is under load should be larger. Even if we assume a several fold increase, the COD under load should not be more than 1 μm.

A polished and etched surface of specimen F41-5 showed dispersed matrix plasticity (Figure 25) in terms of concentrated slip bands. It is important to note that matrix inelasticity was not confined to the tip of fiber cracks only. Slip bands can be observed away from fiber cracks. In F41-6 and F41-7 specimens which were tested and removed after only 3 and 30 cycles, respectively, evidence of slip bands were observed. These are shown in Figures 26 and 27.

An important aspect of our experimental investigation was to understand the nature of fiber crack evolution as a function of TMF cycles. We have already visited what would be a high density of fiber cracks as shown in Figure 15 for a specimen that was cycled to over 7,500 cycles. Specimen F41-6 and F41-7 were tested for 3 and 30 cycles, respectively at 1114 MPa maximum stress.

In Figure 28, we found only a few fiber cracks after 3 cycles, and those occurred exclusively around Mo-weaves. Thus, these locations are prime sites for the initial fiber cracks, possibly through damage of the fiber during consolidation, or through stress buildup at such non-uniform matrix microstructure locations. Note, however, that later cracks occurred away from Mo weaves, indicating that Mo weaves are not a necessary requirement for fiber cracks. In Figure 29, the fiber crack density observed is qualitatively higher for specimen F41-7, which was cycled for 30 cycles. However, the overall number of cracks in this specimen was well below that observed in a specimen that was cycled for the same loading condition to over 7500 cycles (F41-5) and did not fail (Figure 15). These results point to the fact that the *fiber cracking process is a progressive mechanism*, that is, it depends on the number of IP TMF cycles until failure occurs. It

implies that a specimen cycled for many more cycles at the same stress level and temperature cycle compared with another specimen will develop more fiber cracks.

The distributed fiber cracking phenomenon was observed at relatively low applied stresses for specimen F41-17 e.g. at a 700 MPa maximum stress level (Figure 30). At this stress level, if all the load is transferred to the fibers due to matrix stress relaxation, then the maximum fiber stress will be about 1700 MPa. Single fiber tests conducted at NASA-Lewis from the as-received MMC-41 laminate showed a minimum fiber strength of 2250 MPa with the highest fiber strength being 5865 MPa, the average being about 4200 MPa (Figure 31). Thus, fiber failure is not anticipated at 700 MPa maximum applied stress. Fiber strength distribution studies show a wide variation in strength of SCS-6 fibers which in some cases exhibit a bimodal distribution.

To arrive at a threshold stress where no fiber cracks would occur, the maximum applied stress was reduced to 300 MPa. However, distributed fiber cracks were also observed at this stress level, although their density was extremely low. If all the load was taken by the fibers, this stress would imply an average fiber stress of approximately 732 MPa, a level well below any measured strength of fibers. The implication is that a threshold stress may not exist. Consequently, life assessment under IP TMF conditions has to be made based on the fact that fiber cracks will exist, and it must be determined whether the stress levels are high enough to accelerate fiber damage to the point where overload failure can occur within a few thousand cycles. If the kinetics of fiber damage progression are not high enough at that load, then matrix damage will take over, and fiber damage would then play a less critical role.

Because of fiber cracks at low stresses (300 to 700 MPa), it was suspected that the thermal cycling in IP TMF may have an adverse effect on the SCS-6 fibers, particularly through surface degradation or in activating defects in the fiber due to thermal excursion. In order to check whether thermal cycling had a substantial influence on the fiber cracking mechanism, we conducted a number of tests keeping the load constant and imposing thermal cycles between 300-538 C, which was the standard temperature range for all the IP TMF tests. Specimen F41-12 was held at 165 MPa and thermally cycled between 300-538 C for 300 cycles. The specimen was then loaded to 1200 MPa at RT and unloaded. The polished specimen revealed only a few fiber cracks in the gage section (Figure 32). We believe these cracks occurred due to thermal cycling rather than the 1200 MPa tensile load applied at RT, since in our earlier work on monotonic deformation [1,7], fiber cracking was not found to occur away from fracture surface i.e. the distributed cracking mechanism was absent in the monotonic deformation at RT. For the F41-13 specimen, which experienced 300 thermal cycles (300 C-538 C) at a constant applied stress of 700

MPa, distributed fiber cracking was again observed. This test confirmed that thermal cycling had substantial influence on distributed fiber cracking and that pure mechanical cyclic loading was probably not a driver (although it could further accentuate fiber cracking in IP TMF) for the distributed fiber cracks.

To further evaluate whether IP TMF may degrade fibers, we conducted an IP TMF test with a maximum stress of 300 MPa for 300 cycles (Specimen #F41-14). This same specimen was then loaded at RT to approximately 0.8% strain, and then unloaded (Figure 33). Polishing of one face of the entire specimen to the first fiber level showed distributed fiber cracks, although with a reasonable low crack density (Figure 34). At this strain level, the fibers are loaded to about 3000 MPa, and if fibers had degraded, then additional cracks would show up after the RT loading. The other face of the specimen was polished to the ply level after the RT tensile test. Examination of that ply showed no noticeable difference from the fiber crack density before the tensile test. We conclude that IP TMF did not necessarily degrade fibers, otherwise, the magnitude of distributed fiber crack density would be higher after monotonic loading following prior IP TMF loading.

In another aspect of fiber cracking, we had observed that in most cases, the early fiber cracks were located near the Mo weaves (Figures 28 and 29). If Mo-weaves (Figure 35) influenced this cracking mechanism, perhaps as stress concentrators, then their presence could initiate SCS-6 fiber cracks. In order to verify whether Mo-weaves are critical to the initiation of fiber cracks, MMC-30 which were made without the Mo-weaves at NASA-LeRC were tested under IP TMF. Distributed fiber cracking was observed in specimens without Mo-weaves as well (Figure 36) confirming that the distributed fiber cracking mechanism was not unique to laminates with Mo-weaves. In addition, the coplanarity of a few adjacent fibers may be observed in Figure 36, similar to those observed for specimens with the Mo weave. We conclude that distributed cracking, with some coplanarity and possible banding is a characteristic feature of fiber damage under IP TMF loading, independent of the presence of weaves.

The effect of cycle time (16 minutes vs. 2 minutes) was that the slow rate of IP TMF resulted in significantly reduced number of distributed fiber cracks. Figure 37 is for a 16 minute cycle at 700 MPa, and most of the cracks are located along the Mo weave line; cracks were very few away from the weaves. On the other hand, the companion samples with 2 minute cycle time showed significant density of fiber cracks (see Figures 30 and 38). Note again the coplanarity of many cracks. At the slower rate, there is very likely some recovery of the inelastic strain in the unloading part of the cycle which may not occur when the rate of loading is faster. However, this cannot explain the lower crack density for the slower cycles, since the total ratchetting at 200 cycles was actually slightly higher

for the 16 minute cycle than the 2 minute cycle. Rather, explanations need to be sought with regard to the cracking mechanisms. These include possible non-uniform temperature distribution in the composite for the 2-minute cycle, or reduction in stress concentration effects caused by reduced clamping and friction stresses for the longer cycle time. It is useful to point out here that work performed at WPAFB show an opposite effect of IP cycle time, in that a 33-minute cycle produced shorter life than a 2-minute cycle. However, those experiments were performed in air at a higher maximum temperature, and the possible effect of environment on fiber and matrix degradation cannot be ruled out.

A puzzling feature of all the fiber damage was that crack spacings were quite small. In specimens F41-5 and F41-1, with a large number of uniformly distributed cracks, the average fragment length was approximately 600 μm. Using a friction stress of 80 MPa (actually a more appropriate value is about 35 MPa at temperature, based on the work of Eldridge et al. at NASA Lewis), and fiber strengths between 2200 MPa and 5000 MPa, the average fragment length is calculated to be between 1.9 and 2.9 mm, using a simple shear lag analysis. Clearly these numbers are much larger than observed fragment lengths, and suggest that clamping stresses may be much larger with accompanying higher friction stress. The elastic calculations of Nicholas and Ahmad [23] indicate that clamping stresses can be extremely high at a broken fiber tip, implying little or no debonding. Small debond lengths, typically of the order of one fiber diameter, were indeed observed under IP TMF conditions. Thus, the debond and fragment lengths are in qualitative agreement with those of reference [23]. However, for the long cycle times, or under creep conditions, these clamping stresses should reduce substantially, and allow for much larger fragment lengths. Sufficient data were not available to make an assessment of this possibility.

DISCUSSION

Based on our test data and results obtained from testing specimens in an inert atmosphere, it is clear that distributed fiber cracking is an inherent damage mechanism in IP TMF. This damage mechanism can occur independent of oxidation effects. Note that all the tests were performed in a reasonably good inert environment, and that significant fiber damage occurred within a few hours at a reasonably low temperature; based on available data in the literature, little if any fiber damage can occur due to environmental degradation or due to reaction with the matrix under these conditions. Additionally, fiber damage was assessed to be insignificant, based on some of the specific tests undertaken in this study.

Distributed fiber crack density increases as a function of IP TMF cycles and was determined to be a progressive mechanism, as we compared the damage states in specimens F41-6, F41-7 and F41-5. Crack density was progressively higher at 3 cycles (F41-6), 30 cycles (F41-7) and 7500 cycles (F41-5).

We have consistently observed an early maximum increase in strain, typically within the first ten cycles (Figure 11). Given that only a few fiber cracks are likely to occur for a maximum stress of 1114 MPa or less, the early part of the ratchetting response is likely to be the result of viscoplastic deformation by the matrix. The exact degree to which fiber cracks influence the ratchetting response is difficult to ascertain. It is difficult to isolate the fiber crack induced strain increment from the matrix viscoplastic increment because of their complex interaction and the absence of any reliable micromechanics model that accounts for all the nonlinear interactions. However, based on the fiber crack density and the average crack surface displacement, we made some estimations as to what would be an upper bound of strain due to the fiber crack density. The fiber crack density for highly cracked fibers in F41-5 specimen was as high as 10/mm. As an upper bound, if we assume that cracks in adjacent fibers are lined in a series and the deflection along this line is 0.3 μm (although the matrix is not cracked), then the strain in a unit gage length is (0.3 μm x 10)/1 mm = 0.003. Also, during testing, the crack opening displacements are likely to be higher under load. Our estimates are that much of the strain can be accounted for in the strain increase from about 0.007 to 0.01 for the F41-5 specimen due to fiber cracks. However, note that this would be an extreme case since crack density for most fibers will be lower than 10/mm. Also, due to the uncracked matrix between cracked fibers and the probability of finding adjacent fiber cracks along a line, we are unable to precisely estimate the contribution of fiber cracks on ratchetting strain. However, the strain value of 0.003 can serve as an upper bound for this specific case.

An important observation in IP TMF tests was that as a result of loading, there was no appreciable change in the compliance of the specimen. The reported axial fiber modulus (400 GPa) is four times that of the matrix (100 GPa), and it was expected that due to the distributed fiber cracks, significant reduction in stiffness would occur for IP TMF cycles. The work of Varna et al., [29] on the influence of crack-opening displacement of distributed cracks on stiffness loss sheds light on this problem.

The deformational response of a cracked cross-ply laminate (Figure 39) can be expressed in terms of changes in the longitudinal Young's modulus (E_X) as [29]:

$$E_x = E_x^0 - 2E_T \frac{2\eta d}{d+b} U_\alpha \qquad (1)$$

where the superscript o denotes initial value, E_T is the transverse composite modulus, η is the transverse crack density (# of cracks per unit length) and d and b are distances as shown in Figure 37. For a unidirectional MMC, one can redraw Figure 39 in the context of cracks in the fibers, rather than in the 90^o ply as in a cross-ply laminate (Figure 40). For the SCS-6/Ti 15-3 specimens, we have made over fifteen SEM measurements of the crack opening displacement (U_a) with an average of 0.3 μm as COD. In all cases, we found U_a to be at the submicron level. A typical photomicrograph of a fiber crack was shown in Figure 24. For the case of highly distributed fiber cracks, e.g. in F41-5, the crack density is about 10/mm along the fiber length. We considered crack densities up to 100/mm to study a wide range of possible effects. Realistically, the fiber crack density in most fibers will be less than 10/mm. E_x^o is taken to be 200 GPa. The transverse modulus of the MMC is taken to be 125 GPa. The term d/(d+b) represents the volume fraction, which in this case is 0.41. For a series of U_a, we plotted Equation (1) in Figure 41. It is clear that the effect on reduced modulus for U_a =0.3 μm is extremely small. This COD is about 100 times smaller than typical transverse cracks which occur in the 90^o plies in a cross-ply polymeric composite. Therefore, for very small crack opening displacement of transverse fiber microcracks, a reduction in Young's modulus is not expected for the magnitude of the crack density encountered in the MMC specimens in IP TMF. Even for a 1 μm COD, there is no appreciable decrease in modulus as shown in Figure 41.

Examination of IP TMF cycled specimens revealed that there were many uncracked fiber segments that remained as load carrying members (Figures 42 a and b). Furthermore, nonplanar (plane perpendicular to fiber direction) damage in each ply may keep the specimen intact (Figure 43). Residual strength test after 300 cycles at 850 MPa showed that a high residual strength can be maintained (Figure 44). The residual strength of 1300 MPa is close to the original tensile strength of 1400 MPa for MMC-41. Even under the presence of fiber cracks, uncracked high strength fiber segments continue to carry the load. This failure condition for a MMC with cracked fibers is central to Rosen's analysis [30] of unidirectional composites. The statistical fiber failure process described in the analyses of Rosen [30] and Zweben [31] are useful in describing the fiber crack accumulation process in the case of IP TMF. Analysis by He et al [32] is also very useful.

In a composite with broken fibers, the fiber ineffective length (δ_{ineff}) over which the adjacent fiber sees elevated stress is given by [30]:

$$\frac{\delta_{ineff}}{d_f} = \frac{1}{2}\left[\frac{(1-V_f)^{1/2}}{V_f^{1/2}}\left(\frac{E_f}{G_m}\right)\right]^{1/2} \cosh^{-1}\left[\frac{1+(1-\varphi)^2}{2(1-\varphi)}\right] \qquad (2)$$

where V_f = fiber volume fraction, d_f = fiber diameter, E_f = fiber Young's modulus, G_m = matrix shear modulus, and φ = fraction of undisturbed stress value below which fiber is considered to be ineffective. The cumulative fracture propagation mode is presented in Figure 45. It is noted that for a selected composite, the shear modulus, G_m can be affected at temperature for a composite and will influence the ineffective length, δ_{ineff} and consequently increase the zone of stress elevation in the adjacent fiber. Thus, statistical fiber fracture process is favored at elevated temperature once fiber cracks have occurred in a composite system.

An issue at hand is why fiber cracks were observed at low stresses and at mechanical strains as low as 0.5%. At 300 MPa, the cracks were primarily located near Mo weaves, so that some reaction induced damage is a possibility. However, at 700 MPa at 0.0833 Hz, the crack density was significant at locations away from Mo weaves, with some crack coplanarity also being observed (Figures 30 and 38). If all the applied load was taken by the fibers, the fiber stress would only be 1700 MPa, a reasonably small number. It may be recalled that the minimum fiber strength out of a total of forty fibers extracted from the as-received MMC was 2250 MPa; Weibull analysis provided an average strength of 4270 MPa for a 20 mm gage length, and a Weibull modulus of 5.5. At 1700 MPa, this implies a fiber failure probability of only 0.7%, so that if 50 fibers were sampled in a ply, then at most 1 fiber would be found to have failed. Clearly this value is in disagreement with the IP TMF results. One possible explanation, given the observed crack coplanarity of a few adjacent fibers, is that when an isolated fiber fracture does occur, it induces, by stress concentration, failure in adjacent fibers. The exact mechanism for the stress concentration is not clear, nor do we know the value of the stress concentration factor; based on the work of Hedgepeth and Van Dyke [28], we estimate a stress concentration of about 1.25 for three cracked fibers in a hexagonal array. Local pockets are therefore set up around adjacent cracked fibers, where the matrix creep rate is initially higher, which then slowly dissipates the stresses through a creep mechanism to the rest of the MMC. At such a point in time, global load sharing can take over and reduce the incidence of coplanar cracks in adjacent fibers. Under certain probable circumstances, crack coplanarity can be extended over many more fibers, as was illustrated earlier for sample F41-7. The proposed mechanism currently appears to be the only one that can provide any rational explanation for significant fiber cracks at low stresses. It also is in agreement with the 16-minute cycle tests, where the longer times can reduce stress concentration effects and hence result in less fiber fracture, as observed experimentally. However, analyses and additional experimentation is required to confirm this mechanism.

We have performed some creep analyses using the modified Curtin model proposed by Zu and McMeeking [33], to explore how fiber fractures affect ratchetting rates. The model [33] uses the approach of Goto and McLean [34], but incorporates fiber fractures using the analyses of Curtin[35]. An improvement in the analyses here [36] was the incorporation of residual stresses, which were not included in [33]. The details of the analyses are skipped here for the purpose of brevity, however calculations performed in [36] using parametric values of material properties show a significant influence of a characteristic fiber strength, S_C, which depends on the average fiber strength and friction stress. In Figure 46, the creep curve at 538 C obtained from such an analyses is superimposed on the ratchetting curves illustrated earlier in Figure 12. The creep hours were converted to the number of cycles by assuming one cycle was equivalent to creep for half the cycle duration. This is a rather crude approximation, but does shed insight into the ratchetting curves. The bottom solid line corresponds to the creep prediction, based on measured fiber strengths and assuming a friction stress of 35 MPa at 538 C. The parameters in the Norton creep law were: a pre-exponent of $2.1 \times 10^{-15} sec^{-1} MPa^{-4.1}$, and an exponent of 4.1 [4]. It is encouraging to note that the predicted curve in Figure 46 is in reasonably good agreement with the IF data. However, life could not be predicted, since the analyses indicated that creep rates would reduce to zero after a long time. It is also important to note that the creep analyses grossly under-predicted the ratchetting rates for the IP specimens. It was suspected that this under-prediction was due to the fact that possible stress concentration effects were not included in the analyses. As a first approximation in incorporating stress concentration effects, the value of the Sc was reduced gradually from 100% to 80% of its value in a gradual manner. Thus, the prefactor on Sc was taken to be 1.0 until a strain of 0.5%, then it was linearly decreased to 0.8 at 0.75% strain, and then held steady at 0.8 at all higher strains. The value of 0.8 was arrived at based on the analyses of Hedgepeth et al., who calculated a stress concentration factor of 1.25 (=1/0.8) for three adjacent fiber cracks in a hexagonal array. Using this analyses, failure was predicted in approximately 80 cycles, in agreement with some of the data at this stress level (see Fig.46). Additionally, the predicted ratchetting rates were now in better agreement with the IP data.

The analyses above is preliminary, and a more refined version would include usage of a unified viscoplastic model, such as that by Bodner and Partom. However, the first order calculations do suggest that the characteristic strength of the fibers need to be reduced to predict IP TMF life anywhere close to experimental findings. Since the experiments indicated little or no loss in fiber strength following TMF cycling in the inert

environment, the results suggest that stress concentration effects may indeed be important under IP TMF conditions.

The IP TMF fatigue behavior appears to be very similar to what Chiao [37] found in stress-rupture behavior of unidirectional composites (Figure 47). Over the complete range of stresses, the fiber fracture mechanism was found to be operative. This was modeled by Phoenix and Wu [38] as a chain-of-bundles statistical rupture-lifetime model. Lifetime prediction has been attempted using stochastic fracture properties of fibers-typically assumed to be of Weibull distribution. However, the Phoenix and Wu [38] model does not account for the progressive nature of fiber crack development observed in this investigation. Talreja [39] provides such a basis for growth rate of damage in his approach to polymeric composites for a number of specific cases.

Figure 48 illustrates that the creep strain for sample F41-23 did stabilize, as anticipated, at approximately 0.49% strain, and is consistent with all the load being taken up by the fibers. The predictions of Goto and McLean's creep model [34] is also plotted in Figure 48, which indicates that predictions are quite good if fiber fractures do not occur. Metallographic evaluation of the creep sample did however reveal a few fiber cracks, but they were significantly less in number than the IP TMF specimens. To provide some comparison of the ratchetting response, IP specimen F41-17 ratcheted to approximately 0.61% strain (see Table 2), much higher than the 0.49% for the creep specimen. The higher ratchetting strains under IP TMF are consistent with more fiber cracks observed under IP conditions.

CONCLUSIONS

Based on the results of this investigation, the following conclusions can be reached:

1. Distributed fiber cracking is an inherent mechanism in IP TMF in unidirectional SCS-6/Ti 15-3 composites. The mechanism is progressive in that the distributed fiber crack density is cycle dependent, i.e., there is an accumulation process at work which is aided by the complex interaction of viscoplasticity of the matrix and the statistical fiber fracture characteristics.

2. Limited crack coplanarity in adjacent fibers (3-4 fibers) was seen in all specimens. In a few specimens, the coplanarity extended over many fibers (i.e., the cracks were "banded"), and such specimens had short fatigue lives.

The occurrence of crack coplanarity in adjacent fibers suggest possible stress concentration effects.

3. Fiber cracks were found to occur at very low stresses (300 MPa max. stress) in IP TMF. Fiber strength data evaluated at RT cannot explain the fiber cracking at low stresses in IP TMF. There appears to be no threshold applied stress where fiber fractures would not occur under IP TMF.

4. Well-devised IP TMF, creep and constant-load with thermal cycle experiments indicate that the thermal cycling component has a profound influence on initiation and subsequent accumulation of fiber cracks.

5. Controlled experiments indicate little or no loss in fiber strength following IP TMF cycles in an inert environment.

6. The fiber crack opening displacements (CODs) are small (average ~0.30 μm) for the individual fiber cracks. It was shown that for the density of fiber cracks encountered in these specimens, no appreciable change in stiffness was expected because of the very small COD of fiber cracks even after accounting for a several fold increase of the COD when the specimen is under load.

7. Comparison of IP TMF and creep data at 700 MPa, showed that the creep strain saturated to a constant value after 60 hours of creep. On the other hand, the IP specimens showed pronounced ratchetting, and they were accompanied with many fiber fracture. In other words, IP TMF damage is not just a creep effect.

8. At 700 MPa stress, a 16-minute cycle showed significantly less fiber cracks than a 2-minute cycle. The exact reason is not known, but two possibilities include non-uniform temperature distribution at short cycle time, and greater viscoplasticity induced matrix stress relaxation for the 16-minute cycle.

9. Preliminary creep analyses, that accounted for fiber damage, showed reasonable correlation with the ratcheting data of IF tests. However, the predictions were poor for the IP tests. For this type of loading, the fiber

characteristic strength had to be reduced to predict specimen lives. Since special experiments indicated little or no loss in fiber strength, the remaining possibility is that stress concentrations may be involved under IP conditions, which may explain why IP specimens exhibited significant fiber damage.

10. This investigation has identified the basic elements of a mechanism-based IP TMF life prediction model, namely (1) description of statistical aspects of fiber failure, and (2) rate equation of fiber damage (distributed fiber crack accumulation).

ACKNOWLEDGMENT

The authors would like to acknowledge the constant encouragement of Drs. Bradley Lerch (Program Monitor) and Dr. Rod Ellis of NASA-LeRC. Continued discussions with Mr. Michael Castelli of NYMA was very fruitful. The authors are grateful to Mr. Peter Kantzos, Ms. Pamela Brindley and Mr. John Pickens of NASA-LeRC for conducting push-out tests, the fiber strength tests and preparing the MMC plates without any Mo weaves, respectively. Fruitful discussions with Professor Ramesh Talreja of the Georgia Institute of Technology is acknowledged. Mr. Michael Oliver and Mr. Glen Foster of Battelle are acknowledged for their dedicated efforts in testing and in microstructural evaluation.

REFERENCES

1. Majumdar, B. S. and Newaz, G. M., "Inelastic Deformation of Metal Matrix Composites: Plasticity and Damage Mechanisms," Philosophical Magazine, Vol. 66, No. 2, 1992, pp. 187-212.

2. Majumdar,B.S., Newaz, G.M., Brust, F.W.and Ellis, J.R.,"Deformation mechanisms in a Ti-Alloy/SiC Metal Matrix Composite", Proceedings of the VII th. World Conference on Titanium held in San Diego in June 1992, Ed.F.H. Froes, 1993, pp.2609-2616

3. Majumdar, B. S. and Newaz, G. M., "Inelastic Deformation of Metal Matrix Composites: Part I - Plasticity and Damage Mechanisms," NASA contractor Report No. 189095, 1992.

4. Majumdar, B. S. and Newaz, G. M., "Inelastic Deformation of Metal Matrix Composites: Part II - Plasticity and Damage at High Temperature," NASA Contractor Report No. 189096, 1992.

5. Majumdar, B. S., Newaz, G. M. and Brust, F. W., "Constitutive Behavior of High Temperature Composites, Proceedings of ASME Winter Annual Meeting at Anaheim, CA, Eds. B. S. Majumdar, G. M. Newaz and S. Mall, MD-Vol 40, pp 77-90, 1992.

6. Majumdar, B. S., Newaz, G. M. and Ellis, J. R., "Evolution of Plasticity and Damage in Metal Matrix Composites," Metall. Transactions, Vol. 24A, pp. 1597-1610, 1993.

7. Newaz, G. M. and Majumdar, B. S., "Deformation and Failure Mechanisms in MMC," AD-22, ASME Winter Annual Meeting, Atlanta, 1991, pp. 55-66.

8. Brust, F. W., Majumdar, B. S., and Newaz, G. M., "Constitutive and Damage Response of Ti 15-3/SCS-6 MMC," presented at the ASTM Conference on Fatigue and Fracture, Pittsburgh, PA, May 4-5, 1992.

9. Newaz, G. M. and Majumdar, B. S., "Constitutive Response and Inelastic Mechanisms in Unidirectional MMC Lamina Under Compressive Loading," presented at the ASTM Symposium on Life Predictionof Composites, Hilton Head, April, 1994.

10. Newaz, G. M. and Majumdar, B. S., "Inelastic Deformation Mechanisms in SCS-6/Ti 15-3 MMC Lamina Under Compression," NASA Contractor Report 191170, Prepared for Lewis Research Center, under contract NAS3-26494, September, 1993.

11. Majumdar, B. S. and Newaz, G. M., "Isothermal Fatigue Mechanisms in Ti-Based MMC," NASA contractor Report 191181, Cleveland, Ohio, September, 1993.

12. Castelli, M. G. and Ellis, J. R., "Isothermal and Thermomechanical Fatigue Damage/Failure Mechanisms in SCS-6/Timetal 21S $[0/90]_8$ Composite," Presented at Titanium Matrix Composites Workshop II, LaJolla, CA, June 2-4, 1993.

13. Russ, S. M., Nicholas, T., Bates, M. and Mall, S., "Thermomechanical Fatigue of SiC/Ti-24A1-11Nb Metal Matrix Composites," Failure Mechanisms in High Temperature Composite Materials, AD-Vol. 22 and AMD-Vol. 122, Eds. G. K. Haritos, G. Newaz and S. Mall, ASME, New York, 1991, pp. 37-43.

14. Castelli, M. G., "Thermomechanical Fatigue Behavior of SiC SCS-6/Ti 15-3," HITEMP Review, 1990, p. 33-1.

15. Castelli, M. G., Bartolotta, P. A. and Ellis, J. R., "Thermomechanical Testing of High-Temperature Composites: Thermomechanical Fatigue Behavior of SiC(SCS-6)/Ti-15-3," Composite Materials: Testing and Design (Tenth Volume), ASTM STP 1120, Glen C. Grimes, Ed., Philadelphia, 1992, pp. 70-86.

16. Majumdar, B. S. and Newaz, G. M., "Constituent Damage Mechanisms in MMCs under Fatigue Loading, and Effects on Fatigue Life", presented at the Fall TMS/ASM Meeting, Chicago, October, 1994, to be published in Materials Sc. and Engg. J.(1995).

17. Newaz, G. M. and Majumdar, B. S., "Thermomechanical Fatigue Induced Inelastic Deformation Mechanisms in Low and High Volume Fraction Fiber MMCs," ASME Winter Annual Meeting, Chicago, November, 1994.

18. Mirdamadi, M., and Johnson, W. S., "Thermal Mechanical Fatigue of Titanium Metal Matrix Composites: Literature Review and Analysis,: Presented at the ASTM Fourth Symposium on Composite Materials: Fatigue and Fracture, Indianapolis, May 7, 1991.

19. Schubbe, J. J., and Mall, S., "Damage Mechanisms in a Cross-Ply Metal Matrix Composite Under Thermal-Mechanical Cycling," Proceedings of VIII International Conference on Composite Materials, Honolulu, Hawaii, July 15-19, 1991.

20. Majumdar, B. S., and Newaz, G. M., "Thermomechanical Fatigue of an Angle-Ply Metal Matrix Composite," presented at ASTM Third Symposium on Composite Materials: Fatigue and Fracture, Orlando, November, 1989, ASTM STP 1110.

21. Castelli, M., and Ellis, R., "Thermomechanical Fatigue Damage/Failure Mechanisms in Titanium Matrix Composites," NASA Lewis Research Center Review, November 24, 1993.

22. Mall, S., Nicholas, T., Hanson, D. G. and Russ, S. M., "Thermomechanical Fatigue Behavior of a Cross-Ply SCS-6/ß21-S Metal Matrix Composite," ASME MD-Vol. 40, Constitutive Behavior of High-Temperature Composites, 1992, pp. 91-106.

23. Nicholas, T. and Ahmad, J., "Modeling Fiber Breakage in a MMC," to appear in J. of Composites Science and Technology, Dec. 1993.

24. Majumdar, B.S., and Newaz, G.M., "Inelastic Deformation of MMCs: Thermomechanical Fatigue", NASA Report No. CP 19117, pp.36.1-36.12, 1993.

25. Majumdar, B. S. and Newaz, G. M., "Damage Mechanisms under In-Phase TMF for a SiC/Ti-15-3 System", NASA Report No.CP 10146, pp.41.1-41.13, 1994.

26. Newaz, G. M. and Majumdar, B. S., "Progressive Damage Mechanisms in MMC Under In-Phase TMF Loading," Presented at the 12th ASTM Conference on Testing and Design, Montreal, May, 1994, to appear in an ASTM STP.

27. Sattler, M. L., Kinney, J. H., Zywicz, E., Alani, R. and Nichols, M. C., "The Microstructures of SCS-6 and SCS-8 SiC Reinforcing Fibers," Ceramic Engg. Soc. Proceedings, Vol. 13, #7-8, 1992, pp. 227-237.

28. Hedgepeth, J.M., and Van Dyke, P.,"Local Stress Concentration in Imperfect Filamentary Composite Materials", J. Composite Materials, Vol.1, 1967, pp.294-309.

29. Varna, J., Berglund, L. A., Talreja, R. and Jakovics, A., "A Study of Opening Displacement of Transverse Cracks in Cross-Ply Laminates," International Journal of Damage Mechanics, Vol. 2, July, 1993, pp. 272-289.

30. Rosen, B. W., "Tensile Failure of Fibrous Composites," AIAA Journal, Vol. 2, #11, 1964, pp. 1985-1991.

31. Zweben, C., "Tensile Failure of Fiber Composites," AIAA Journal, Vol. 6, #12, 1968, pp. 2325-2331.

32. He, M.Y., Evans, A.G. and Curtin, W. A., " The Ultimate Tensile Strength of Metal and Ceramic Matrix Composites", Acta Metall. Mater., Vol. 41, #3, 1993, pp. 871-878.

33. Zu, Z.Z., and McMeeking, R.M., "Creep Models for Metal Matrix Composites with Long Brittle Fibers", Submitted to J. Mech. Phys. of Solids, 1994

34. Goto, S.,and McLean, M.,"Role of Interfaces in Creep of Fiber-Reinforced Metal Matrix Composites - I, Continuous Fibers", Acta metall., Vol.39, No.2, pp.153-164, 1991

35. Curtin, W.A., "Theory of Mechanical Properties of Ceramic Matrix Composites", J. Amer. Cer. Soc., Vol.74, p.2837, 1991

36. Majumdar, B.S., Unpublished research, 1994

37. Chiao, T. T., "Some Interesting Mechanical Behaviors of Fiber Composite Materials," in Fracture of Composite Materials, ed. G. C. Sih and V. P. Tamzus, Proceedings of the First USA-USSR Symposum on Fracture of Composite Materials, Sizthoff and Noordhoff, The Netherlands, 1979, pp. 385-392.

38. Phoenix, S. L. and Wu, E. M., "Statistics for the Time Dependent Failure of Kevlar-49/Epoxy Composites: Micromechanical Modeling and Data Interpretation," Mechanics of Composite Materials - Recent Advances, ed. Z. Hashin and C. T. Herakovich, Proc. of the IUTAM Symposium on Mechanics of Composite Materials, Pergamon Press, New York, 1982, pp. 135-162.

39. Talreja, R., Fatigue of Composite Materials, Technomoc Publishing Co., Lanacaster, Pennsylania, 1987.

TABLE 1. SEQUENTIAL IN-PHASE TMF TESTS

	Specimen No.	Max. Stress	Life (Cycles)
Higher Stress Tests	F41-1	1114 MPa	94.5
	F41-2	850 MPa	8161 (DNF)
	F41-3	1000 MPa	4751 (DNF)
	F41-4	1114 MPa	3895
	F41-5	1114 MPa	7511 (DNF)
	F41-6	1114 MPa	3 (DNF)
	F41-7	1114 MPa	30 (DNF)
	F41-8	1114 MPa	52
Lower Stress Tests	F41-9	700 MPa	1000, extensometer data problem
	F41-10	700 MPa cycle time = 16 min	213 (DNF)
	F41-11	Tensile Test	Monotonic
	F41-12	165 MPa, const.	300 (DNF), tensile tested to 1200 MPa and unloaded
	F41-13	700 MPa, const.	300 (DNF)
	F41-14	300 MPa	300, tensile tested to 0.8%
	F41-15	400 MPa	3300, stopped test (strain decrease)
	F41-16	Tensile test up to 0.9% strain unloaded	Monotonic
	F41-17	700 MPa	200 (DNF)
	F41-18	700 MPa cycle time = 16 min	200 (DNF)
Confirmatory Tests	F41-19	1114 MPa	15
	F41-20	1114 MPa	36
	F41-21	700 MPa	200 (DNF)
	F41-22	1000 MPa	500, test problem
	F41-23	850 MPa	300, pulled to failure (1314 MPa residual strength)
	F41-24	700 MPa creep	60 hrs
	B1-1	Tensile	Monotonic
	B1-2	512 MPa	300 (DNF)
	B1-3	512 MPa cycle time = 16 min	300 (DNF)

- DNF = did not fail
- R-ratio = 0.1 for all tests
- IF test was run at 538 C.
- All IP TMF tests were run between 300-538 C and for cycle time 120 sec unless noted.
- Tensile tests conducted at room temperature (RT)
- F41 specimens are with Mo-weave
- B1 specimens are without Mo-weave

TABLE 2. IN-PHASE TMF AND IF TEST DATA AND DAMAGE STATES

(Cycle Times 120 sec except as noted)

Type of Loading	Specimen No.	Maximum * Stress, MPa	Strn Rng, Mech., %	Max. mech. strn. at failure, %	Cycles to Failure	Damage State (Fiber Cracks)
MMC-41, 120 sec cycle time						
IF	F41-4	1114	0.565	0.75	3895	Distributed fiber cracks, and matrix cracks
IP	F41-1	1114	0.63	1.05	94.5	Lots of distributred cracks with some banding
IP	F41-5	1114	0.58	1.00	7516, DNF	Lots of distributed cracks
IP	F41-6	1114	0.58	0.80	3, DNF	Very few cracks around Mo weave
IP	F41-7	1114	0.54	0.81	30, DNF	Distributed cracks with significant banding
IP	F41-8	1114	0.61	0.95	52	ditto
IP	F41-20	1114	0.62	--	36	Not polished
IP	F41-3	1000	0.54	0.92	4751, DNF	Distributed cracks, have interface measurements
IP	F41-2	850	0.46	0.70	8161, DNF	Distributed cracks; Mo-weave effect illustrated
IP	F41-23	850	0.48	0.72	300, DNF	Residual RT strength of 1314 MPa
IP	F41-9	700	--	--	1000, DNF	Not polished
Thermal	F41-13	700, constant	--	0.64	300, DNF	Distributed fiber cracks
IP	F41-17	700	0.38	0.61	200, DNF	Distributed fiber cracks
Creep	F41-13	700	0.38 on reaching full load	0.49	60 hrs, DNF	Few fiber cracks
IP (16 min cycle)	F41-10	700	0.39	0.70	213, DNF	No cracks
ditto	F41-18	700	--	--	200, DNF	Few, but much less than 120 sec cycle
IP	F41-15	400	--	--	3300, DNF	Not polished
IP	F41-14	300	0.17	0.33	300, DNF	Some distributed cracks; subsequent tensile test did not increase number of cracks
IP	B1-2	512	--	--	300, DNF	Some distributed cracks
IP (16 min cycle)	B1-3	512	--	--	300, DNF	Much less cracking than B1-2

* R-ratio was 0.1 in all tests. All experiments were performed in an inert environment.
DNF = did not fail and the specimen was unloaded.
There were additional tests which included tension tests at RT and 538 C, thermal cycling at 165 MPa, and a few extra tests at 700, 1000 and 114 MPa.
B1 specimens are MMC-30 specimens without any Mo-weave.

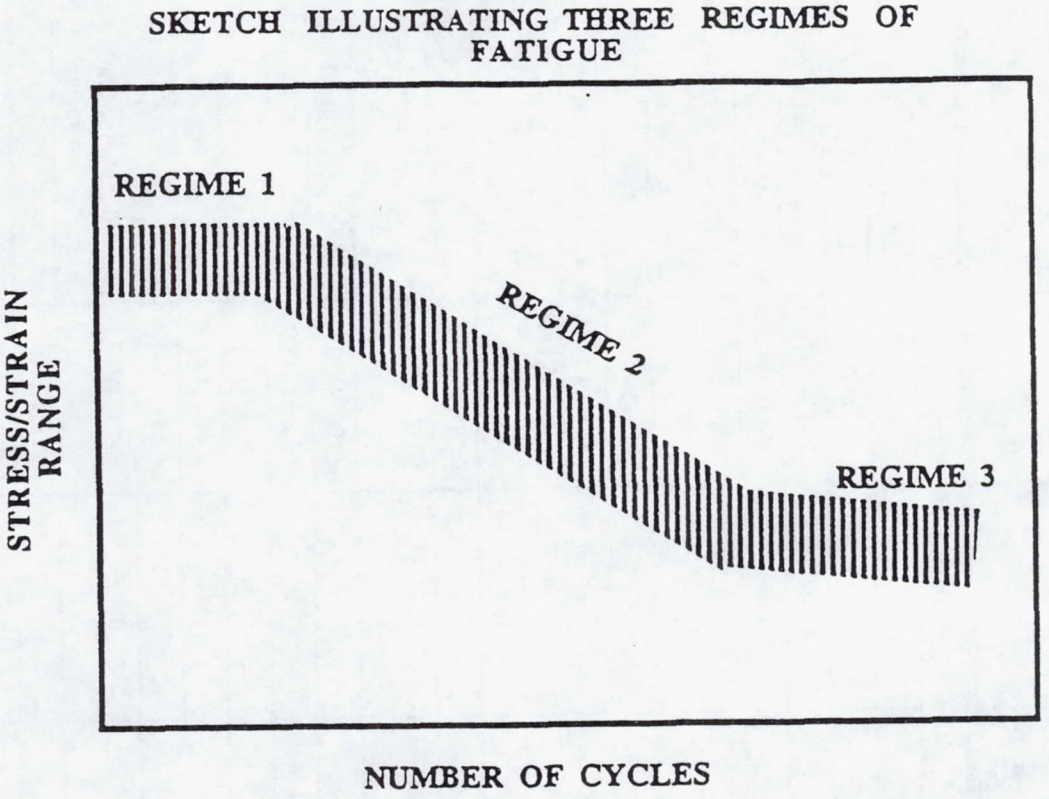

Figure 1. Fatigue life regimes.

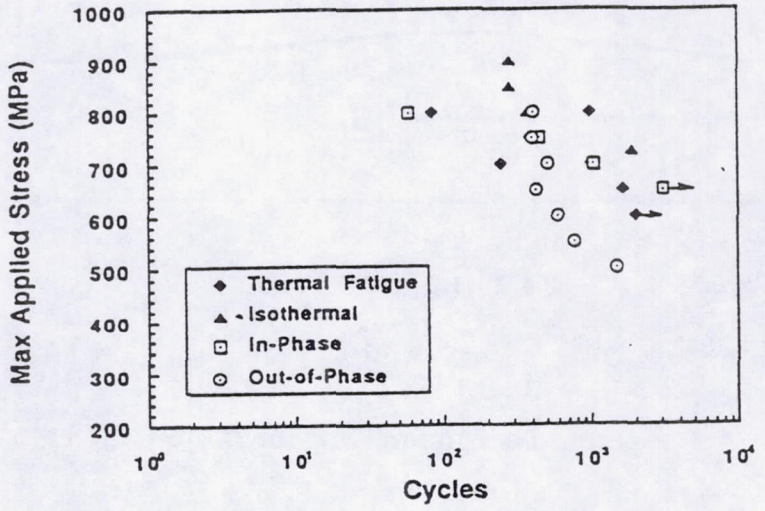

Figure 2. Fatigue life as a function of maximum applied stress for unidirectional SCS-6/Ti 24-11. TMF cycles are 150-650 C, R = 0.1. Isothermal tests are at 650 C [14].

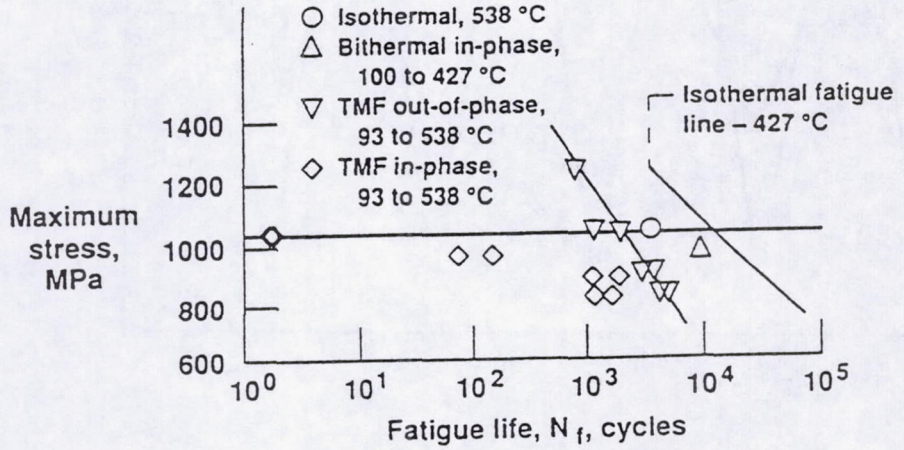

Figure 3. Thermomechanical fatigue results for SiC/Ti-15-3, $[0]_9$ lamina [15].

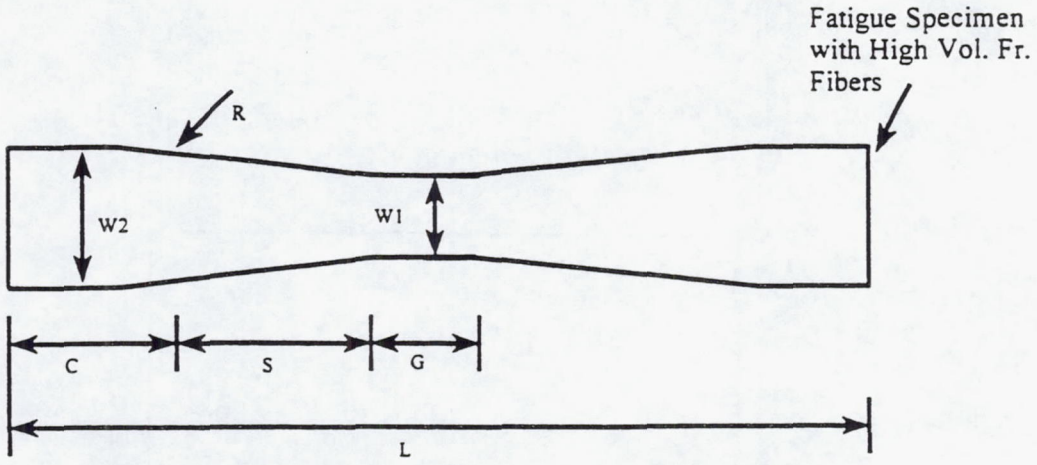

W1 = 0.350"; W2 = 0.472" (1.2 cm); G = 0.720";

S = 1.308"; C = 1.0"; L = 5.35" R = 14"

Figure 4. Specimen design for TMF specimens [11].

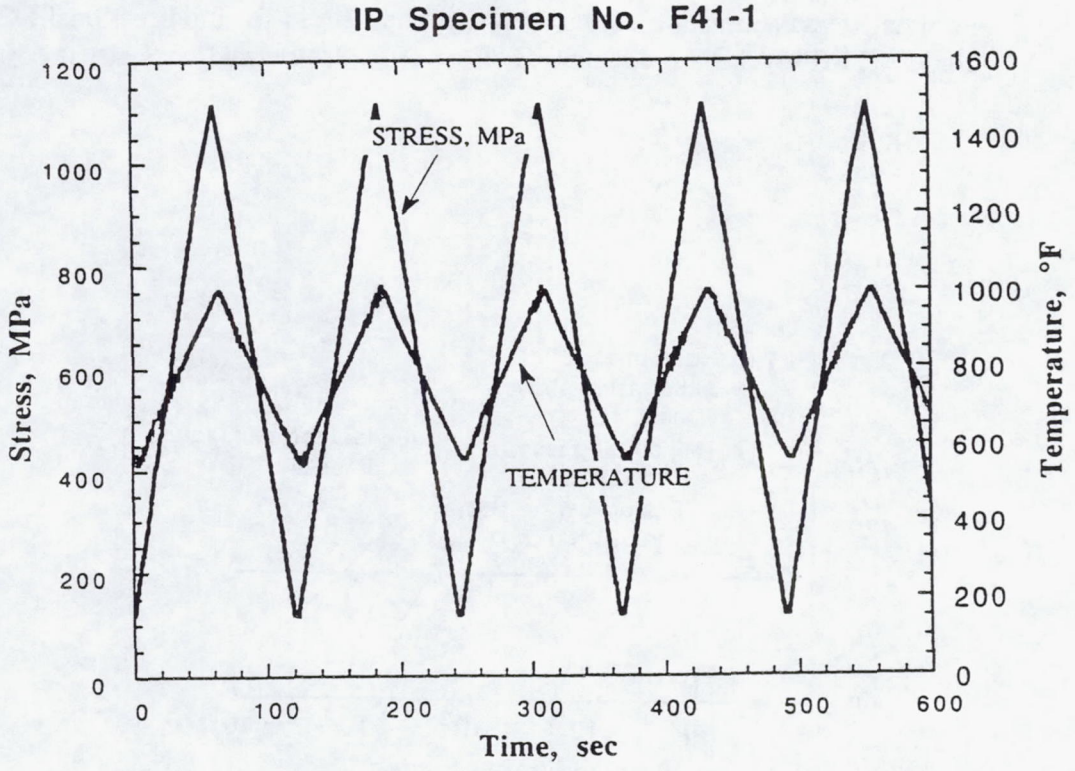

Figure 5 In-phase thermal and stress cycles (command signal) in IP TMF tests.

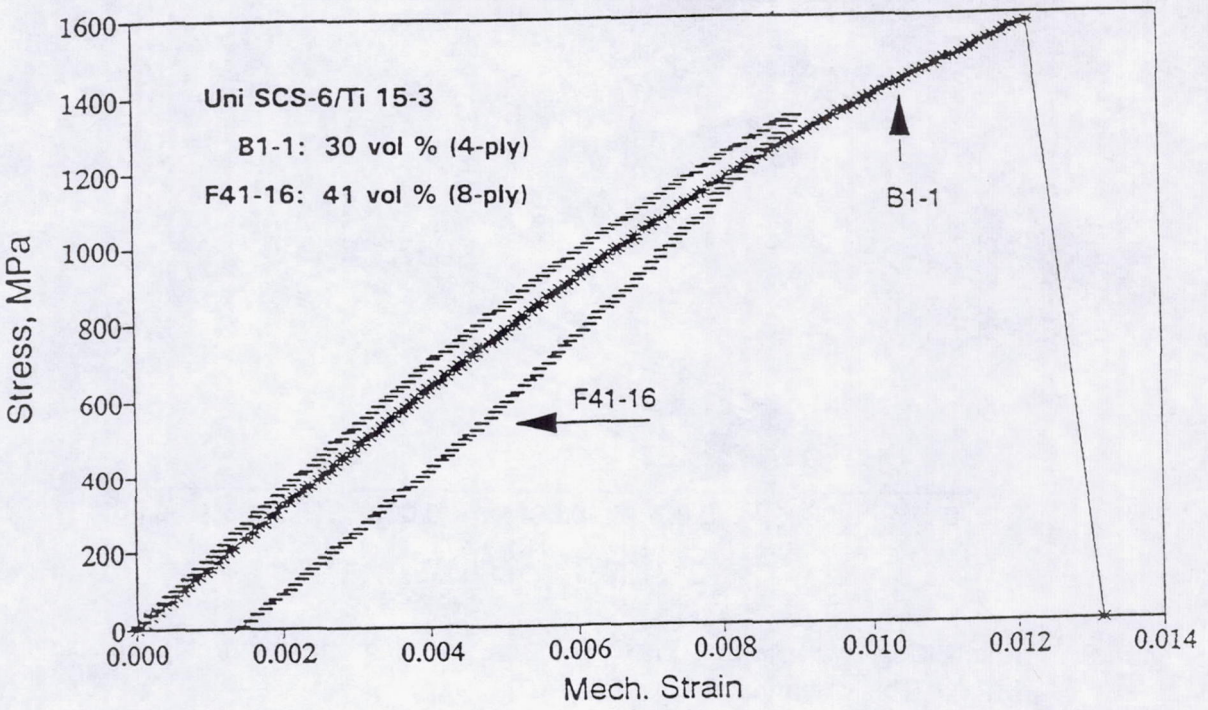

Figure 6. Longitudinal mechanical response of 41 vol % and 30 vol % MMCs.

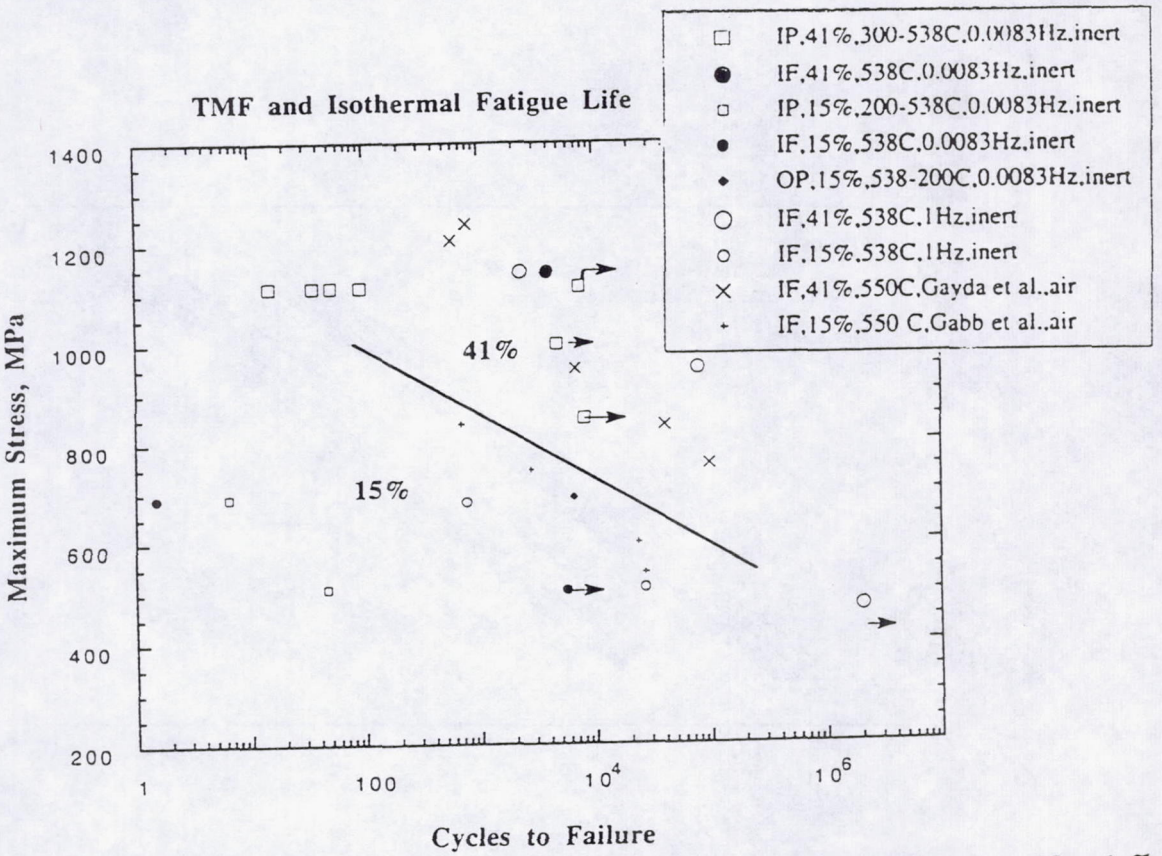

Figure 7. IF and TMF lifetime plot. Includes data from other investigations. 15 vol % MMC data is included. The solid line is a demarcation line between 15% and 41% data. Out-of-phase (OP) data for 15 vol % MMC.

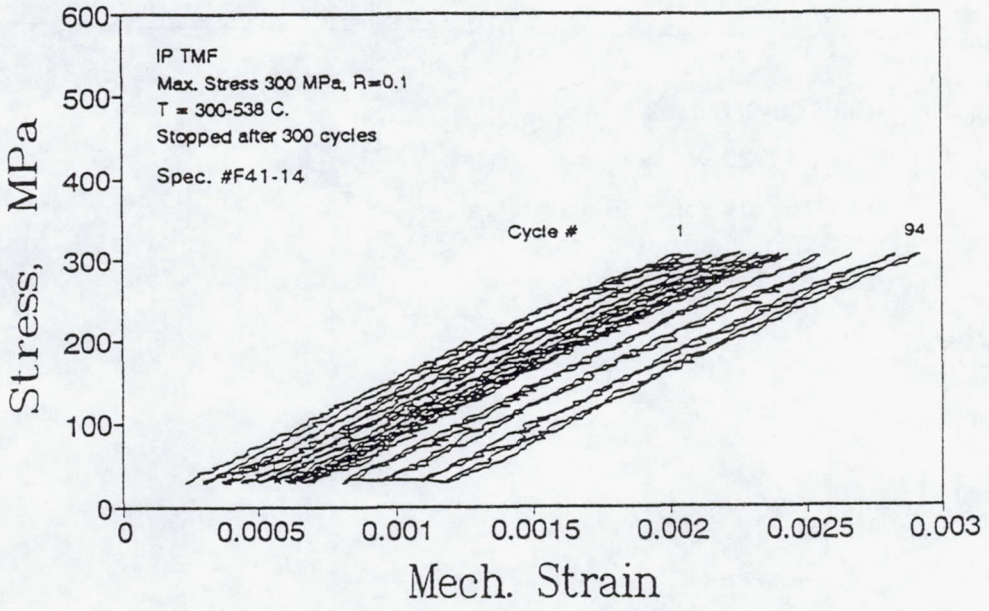

Figure 8. Ratchetting response in a TMF specimen with low maximum applied stress (300 MPa). The specimen did not fail.

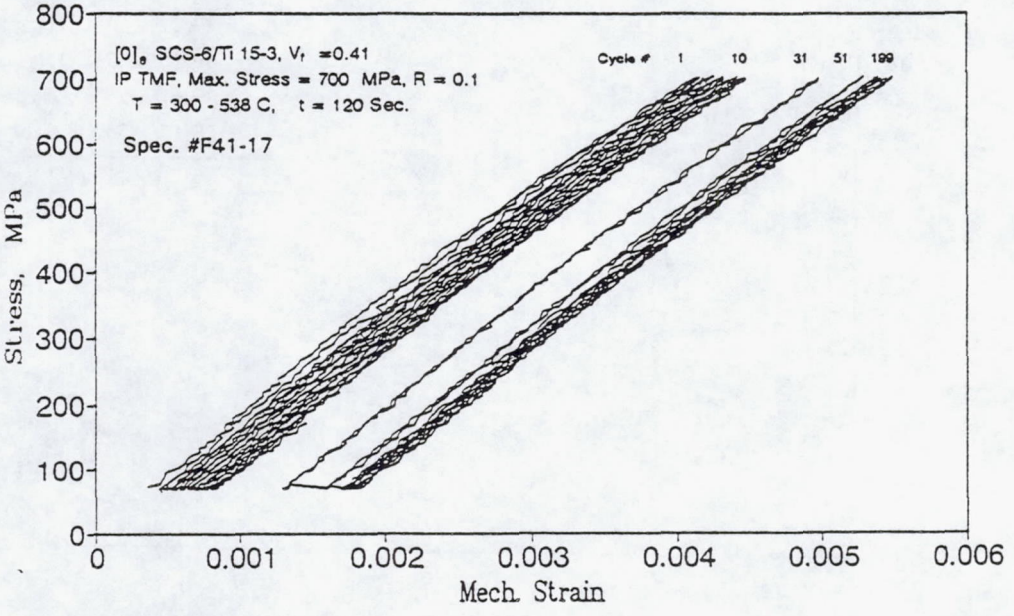

Figure 9. Ratchetting response in a TMF specimen with medium maximum applied stress (700 MPa). The specimen did not fail.

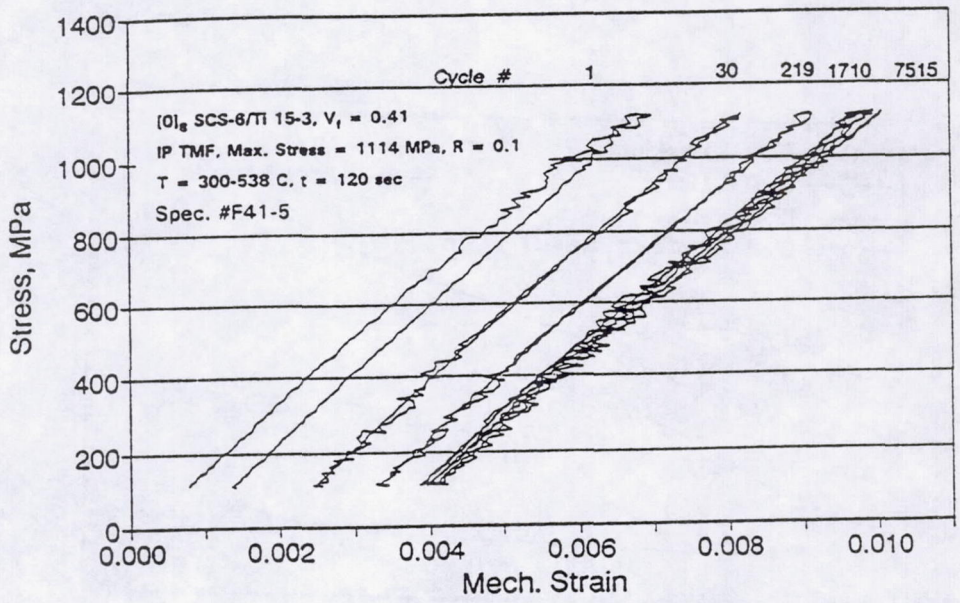

Figure 10. Ratchetting response in a TMF specimen with high maximum applied stress (1114 MPa). The specimen did not fail.

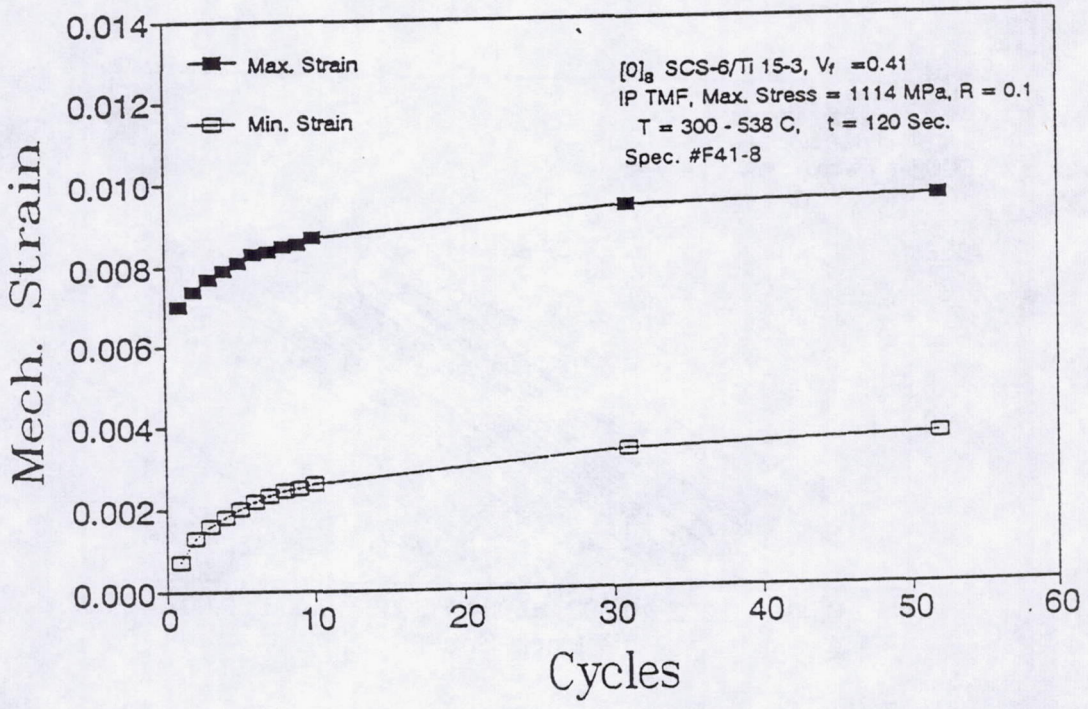

Figure 11. Early strain rise in an IP TMF specimen at 1114 MPa max. applied stress.

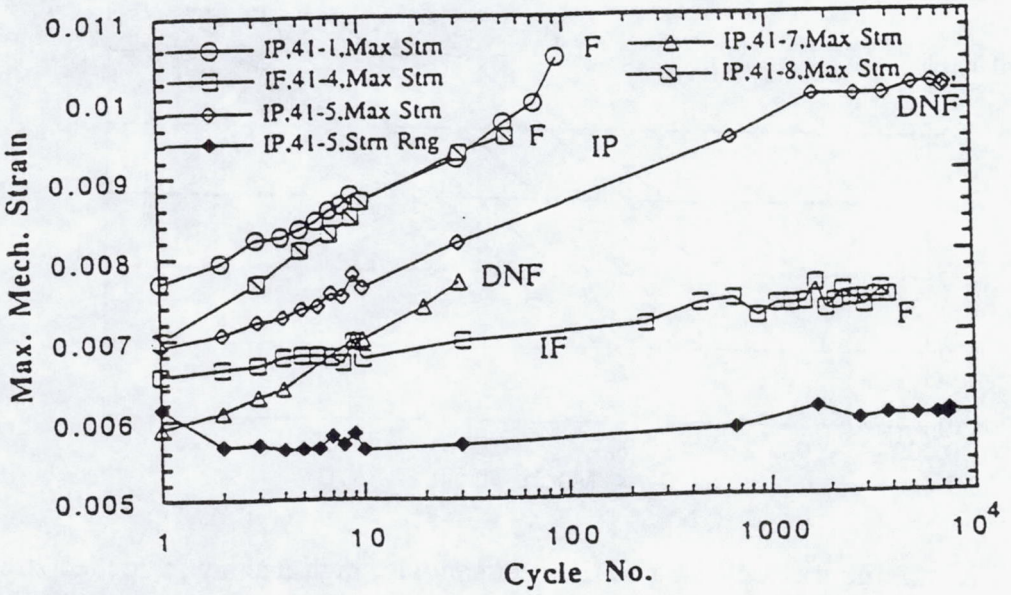

Figure 12. Ratchetting behavior for IP (300-538 C) and IF (538 C) loading; stress range 114-1114 MPa.

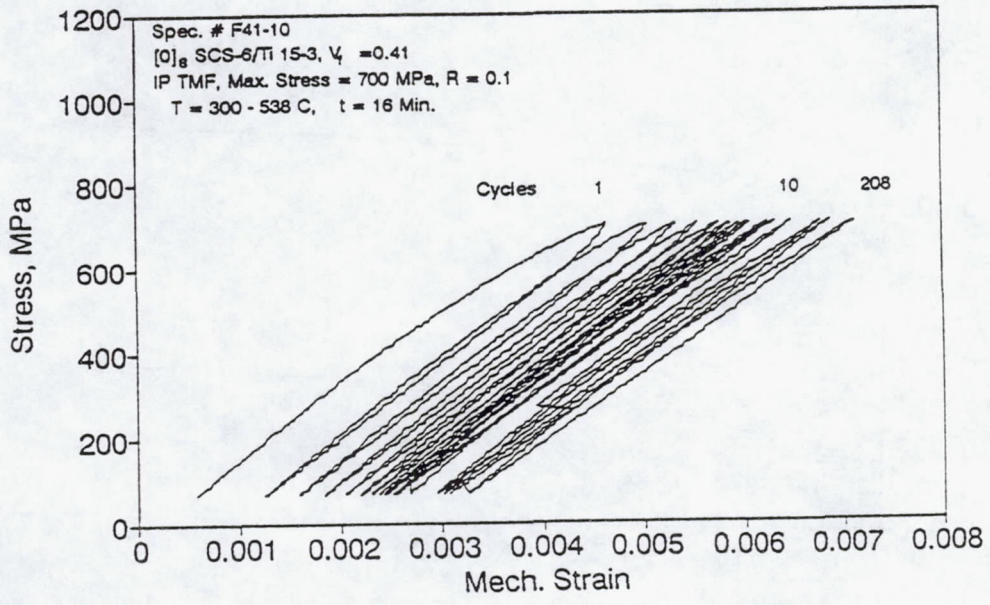

Figure 13. TMF cyclic response for 16 min cycle specimen showing significant nonlinearity on the loading part of cycle.

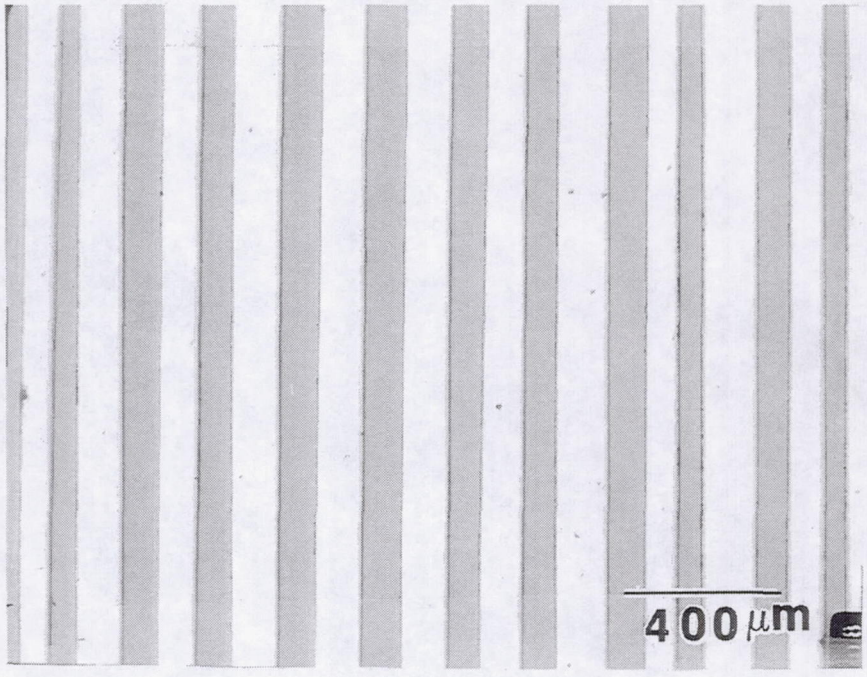

Figure 14. An untested as-polished specimen showing absence of fiber cracks.

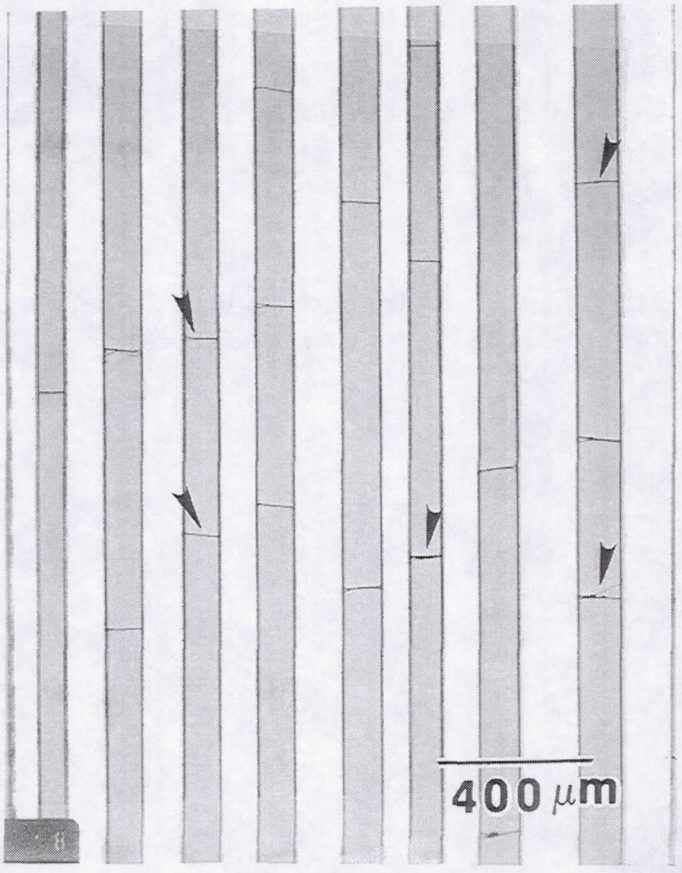

Figure 15. Distributed fiber cracking in IP TMF specimen (F41-5) with max. stress of 1114 MPa for over 7,500 cycles.

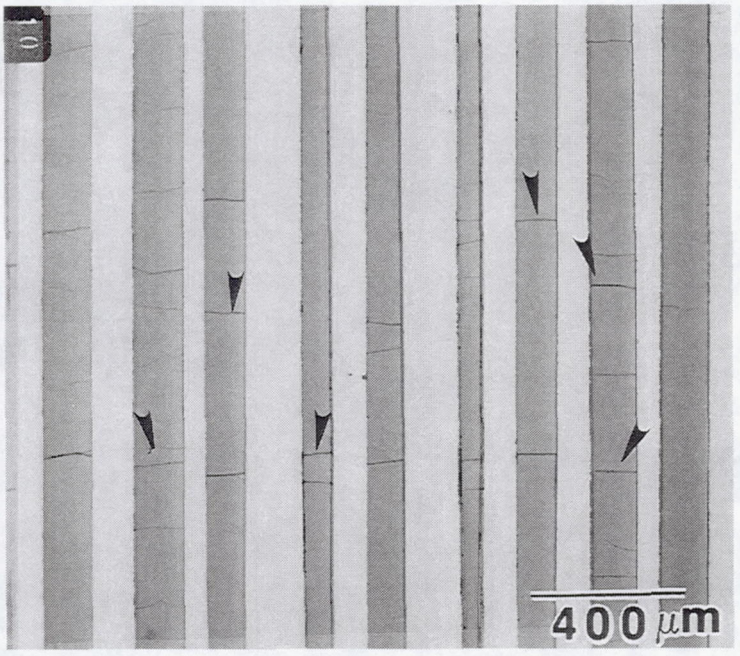

Figure 16. Second level fiber cracks (subsurface) in an IP TMF specimen (F41-5) with max. stress of 1114 MPa for over 7,500 cycles.

FIBER CRACK DISTRIBUTION IN
IN-PHASE TMF
300-538 C, 111-1114 MPa, Unloaded after 30 Cycles
Specimen No. 41-7

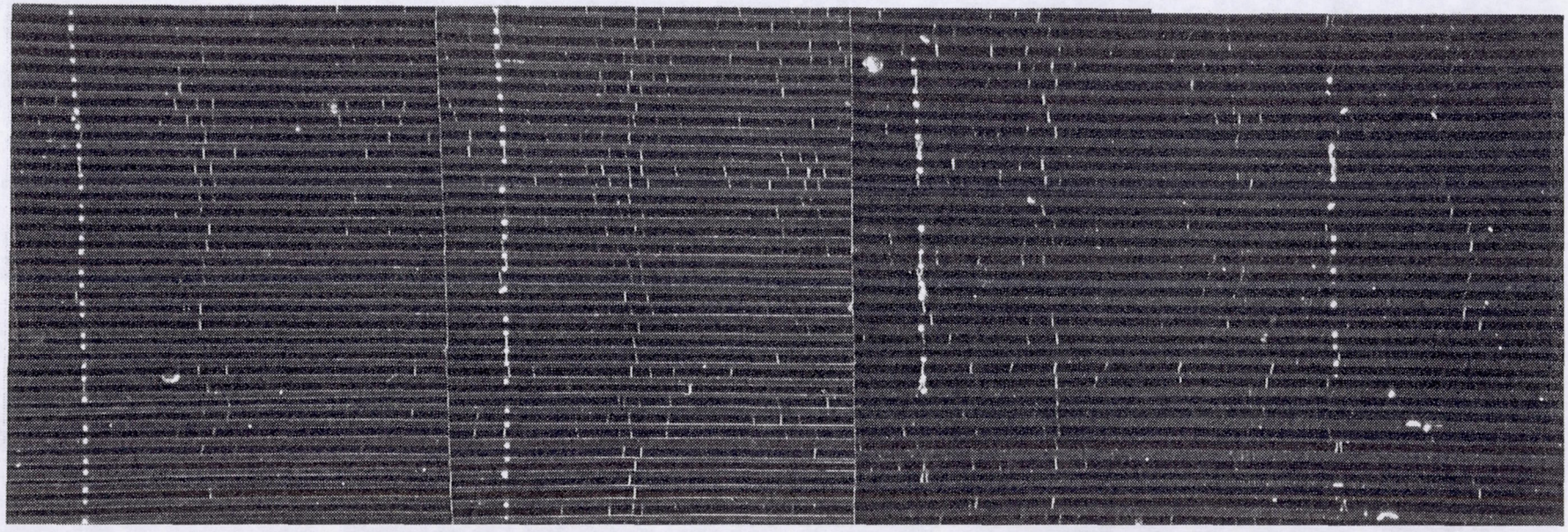

Figure 17. Banding of fiber cracks in specimen F41-7.

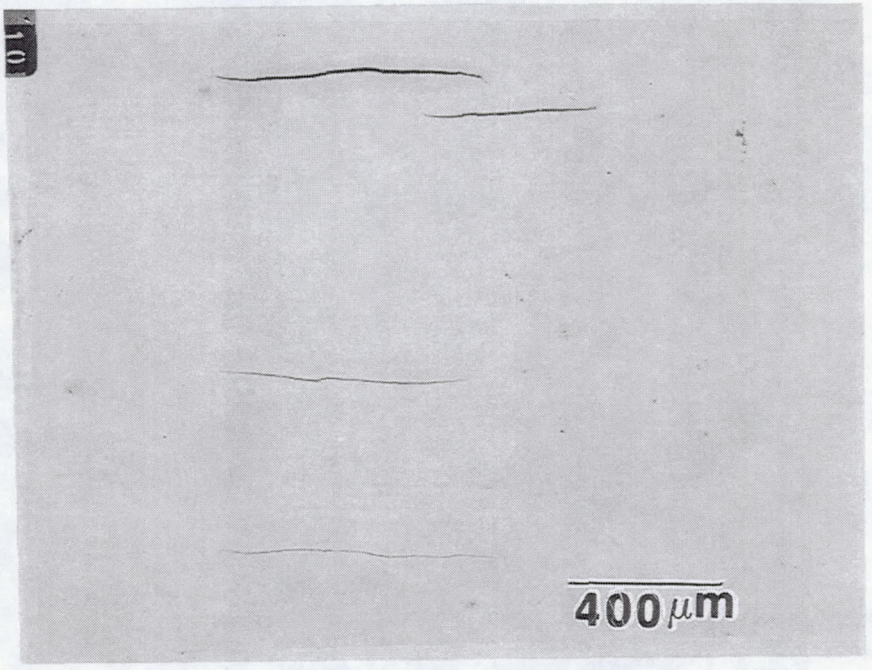

Figure 18. Surface matrix cracks in F41-4 isothermal fatigue (IF) specimen.

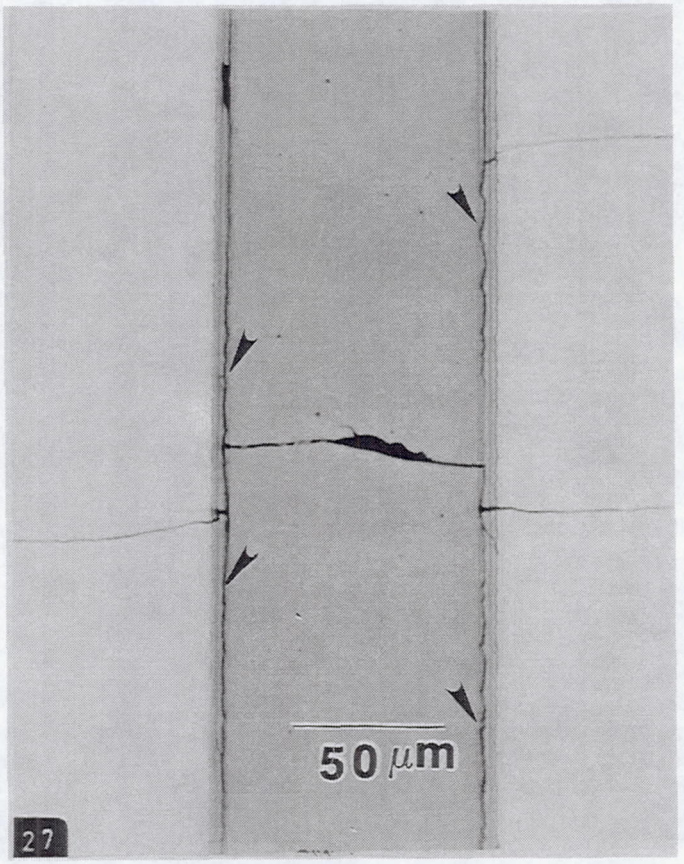

Figure 19. Fiber crack and neighboring matrix cracks in IF F41-4 specimen. Interfacial debonding at SiC fiber and inner coating is also evident (arrows).

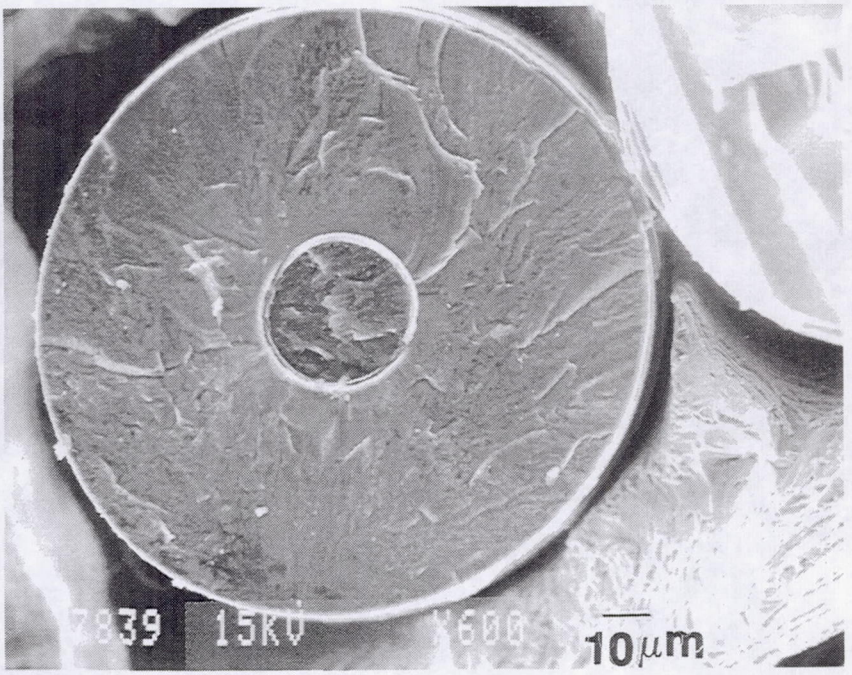

Figure 20. Surface initiated fiber fracture in IP TMF (F41-5 specimen).

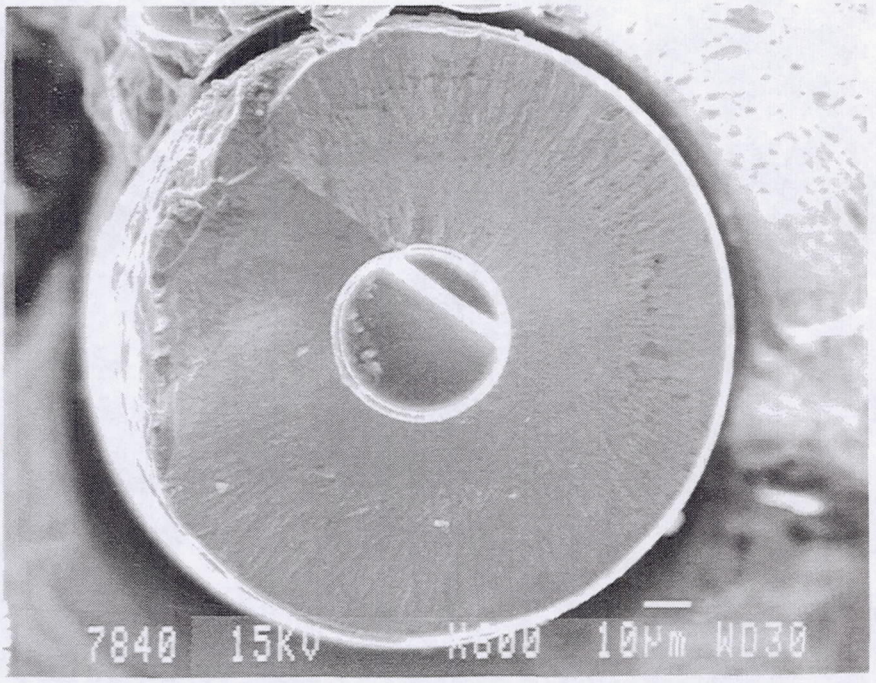

Figure 21. Fiber core initiated fracture in IP TMF (F41-5 specimen).

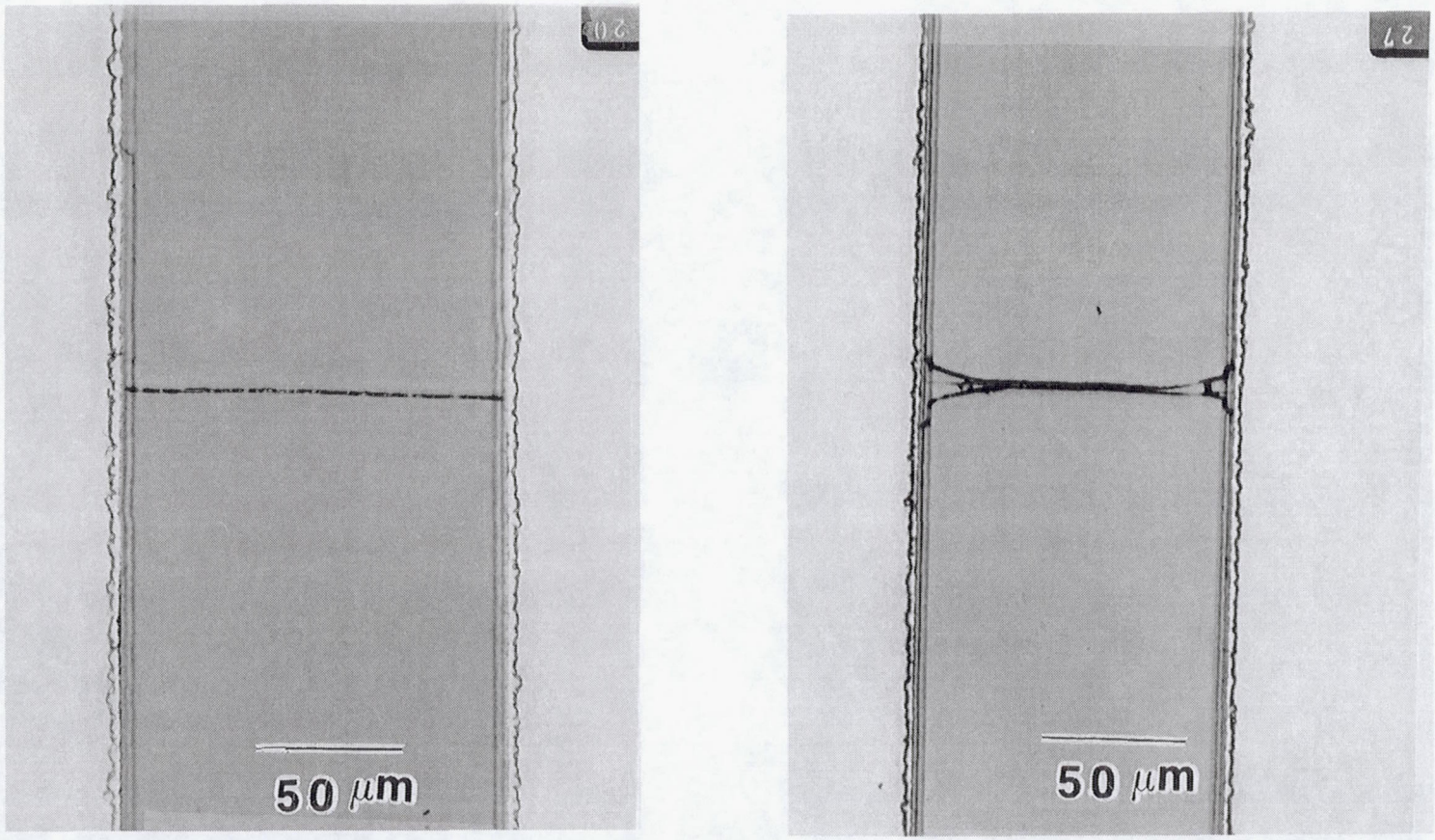

(a) (b)

Figure 22. (a) Single and (b) "Shatter Cracks" in fibers with due to IP TMF loading (F41-5 specimen).

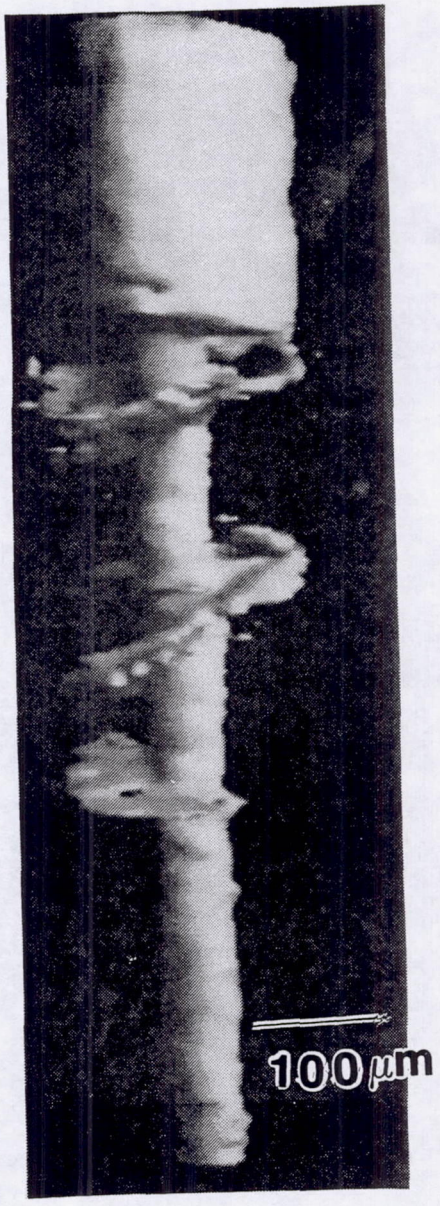

Figure 23. Spiral crack in SCS fiber taken at LLNL [27]. X-ray micrograph of internal fracture surface in an aluminum matrix/SCS-8 fiber composite failed in tension.

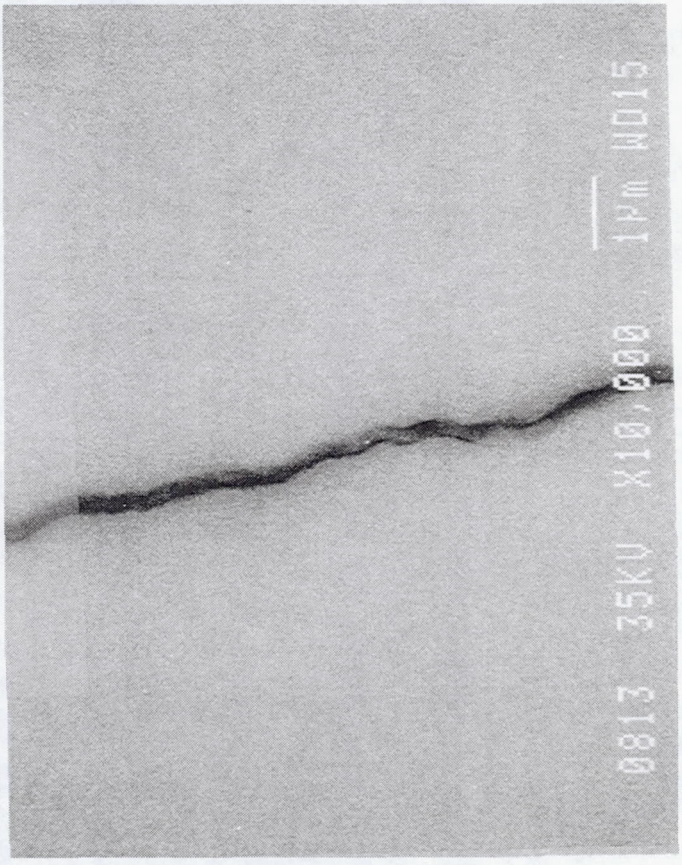

$U_\alpha = 0.3\ \mu m$

Figure 24. Typical COD ($\sim 0.3\ \mu m$) of fiber cracks in a IP TMF specimen.

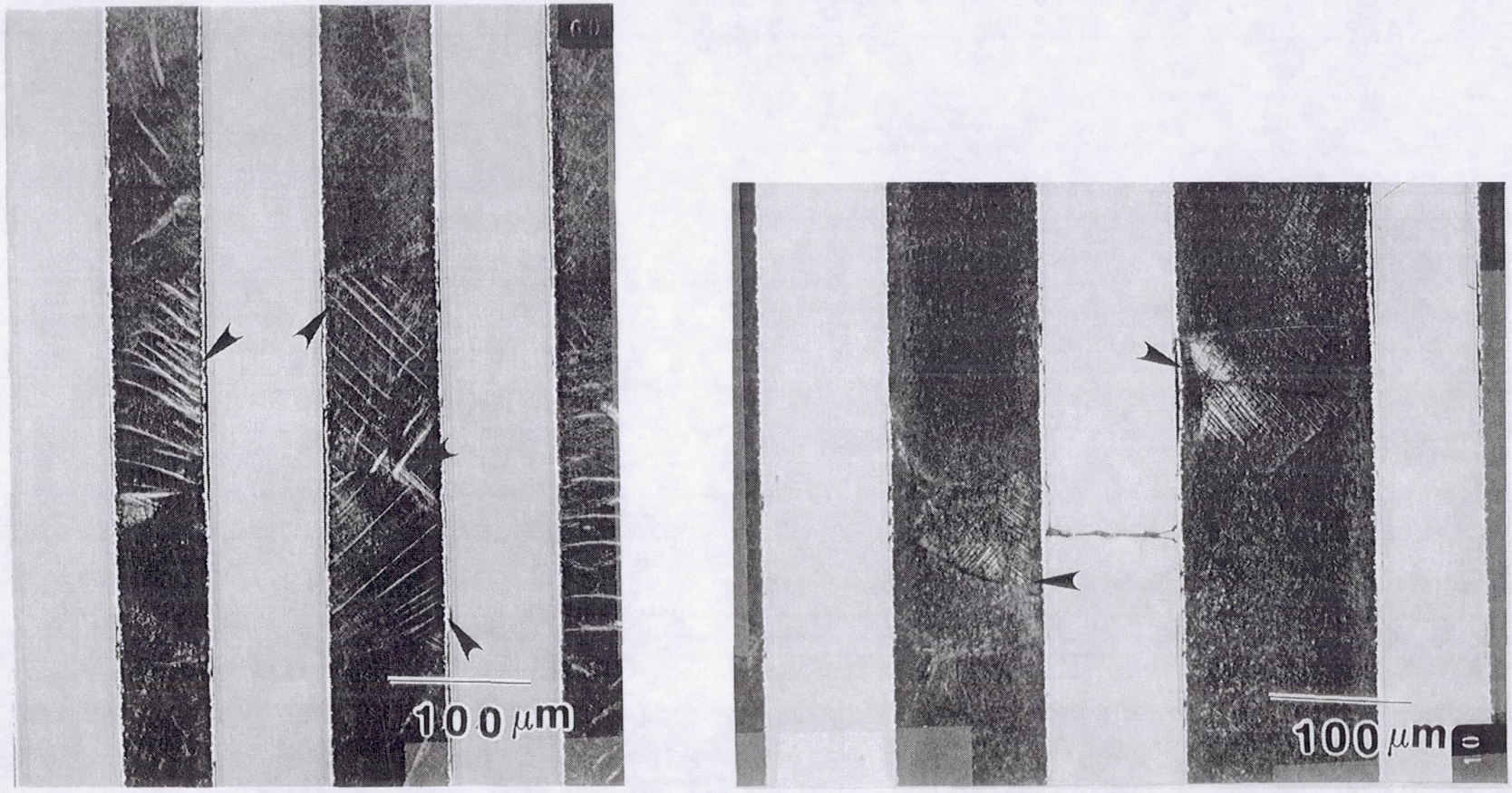

(a) (b)

Figure 25 a,b. Concentrated slip zones in matrix in F41-5 IP TMF specimen.

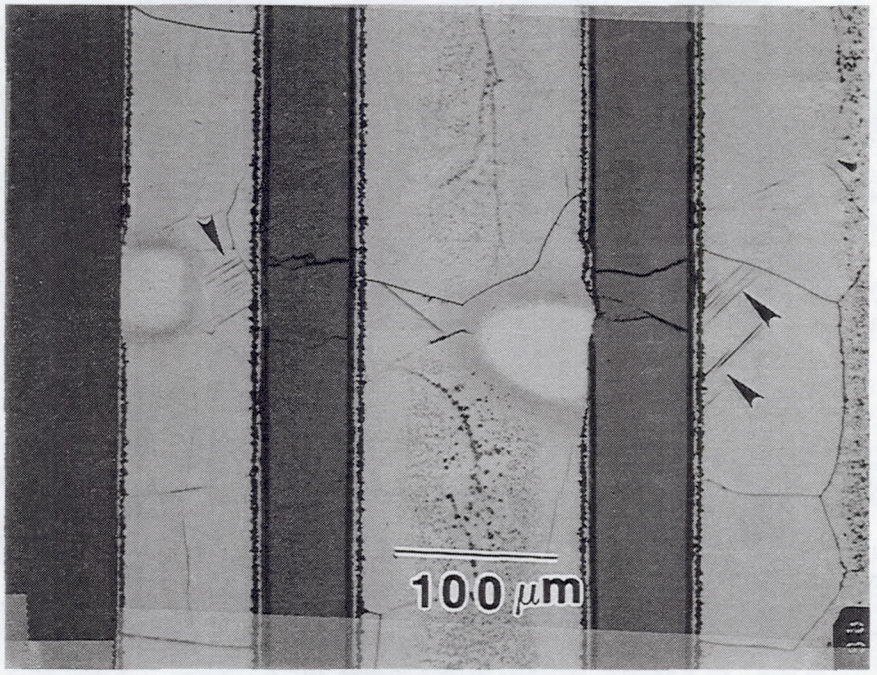

Figure 26. Evidence of matrix plasticity after 3 TMF cycles in specimen F41-6.

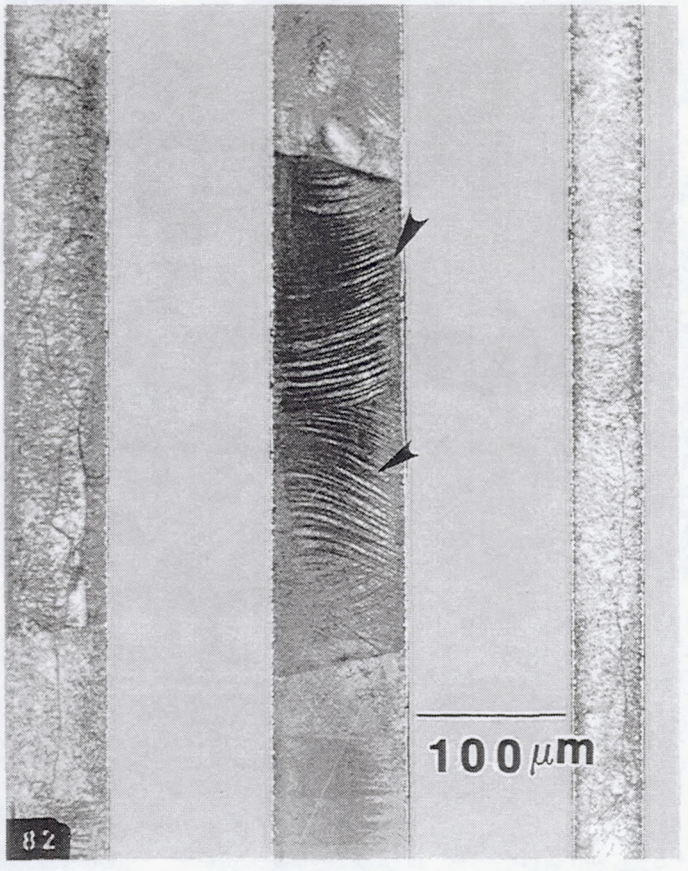

Figure 27. Evidence of matrix plasticity after 30 cycles in specimen F41-7.

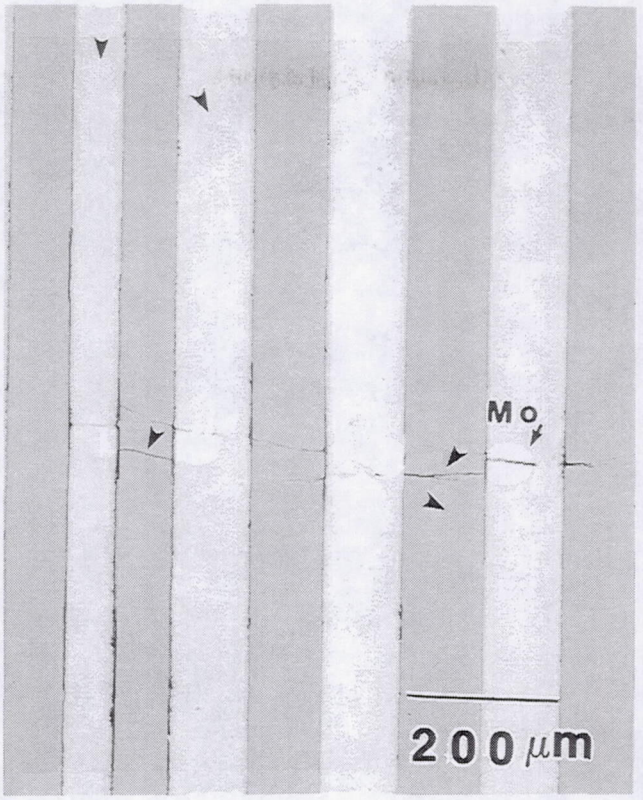

Figure 28. Fiber cracks in F41-6 IP TMF specimen after 3 cycles showing cracks confined to Mo-weave only.

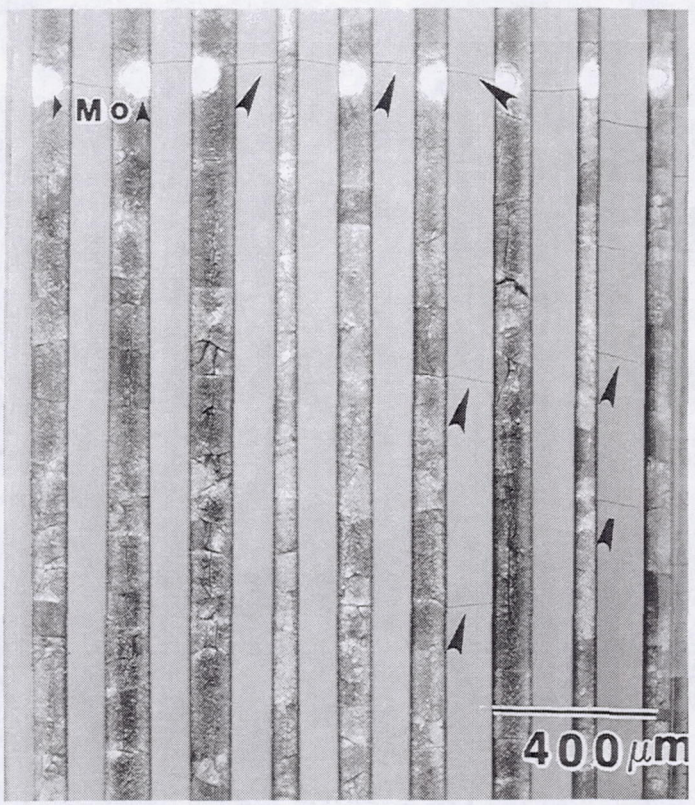

Figure 29. Fiber cracks in F41-7 IP TMF specimen after 30 cycles showing cracks at Mo-weaves and away from it.

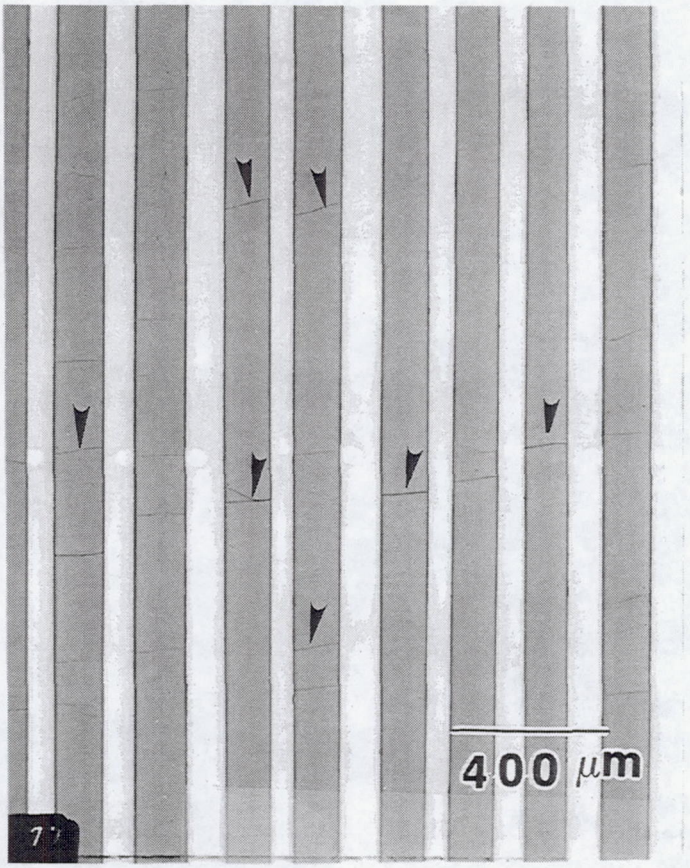

Figure 30. Distributed fiber cracks in a specimen (F41-17) cycled for 200 IP TMF cycles at 700 MPa max. stress.

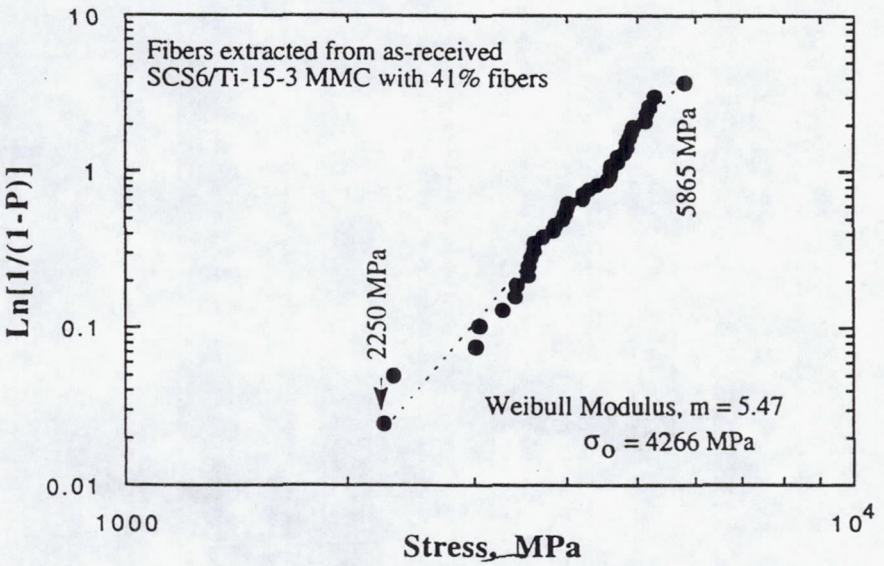

Figure 31. Fiber strength data for fibers extracted from as-received MMC-41 panel.

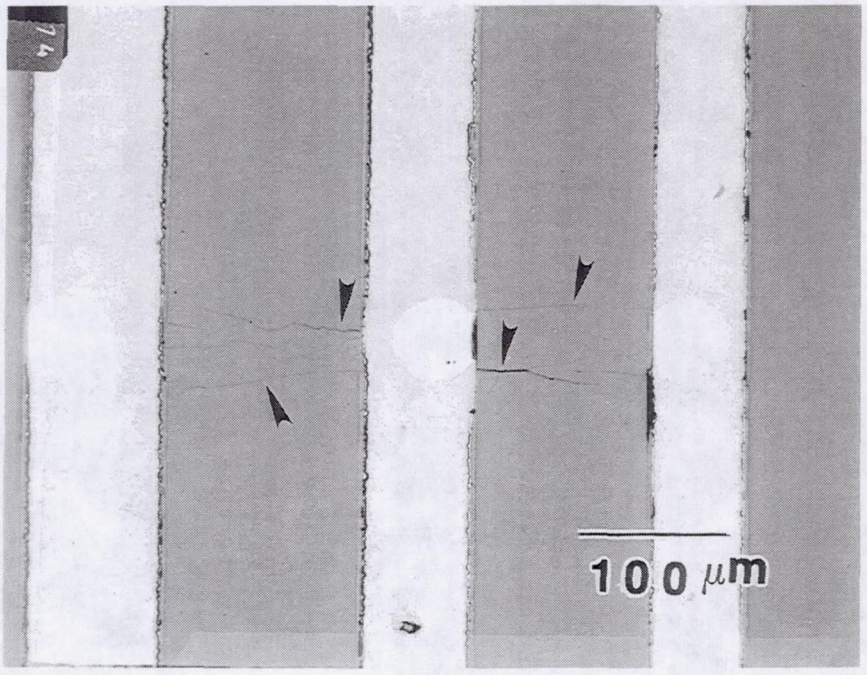

Figure 32. Specimen F41-12 held at 165 MPa constant load and thermally cycled between 300-538 C for 300 cycles and tensile loaded to 1200 MPa and unloaded.

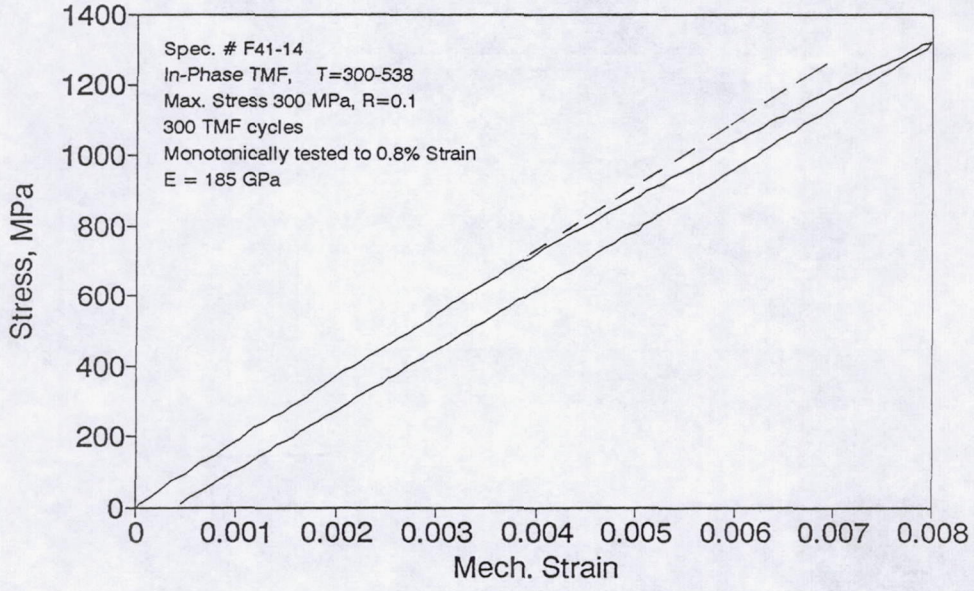

Figure 33. Monotonic response of F41-14 after being subjected to IP TMF cycles with 300 MPa max. stress for 300 cycles.

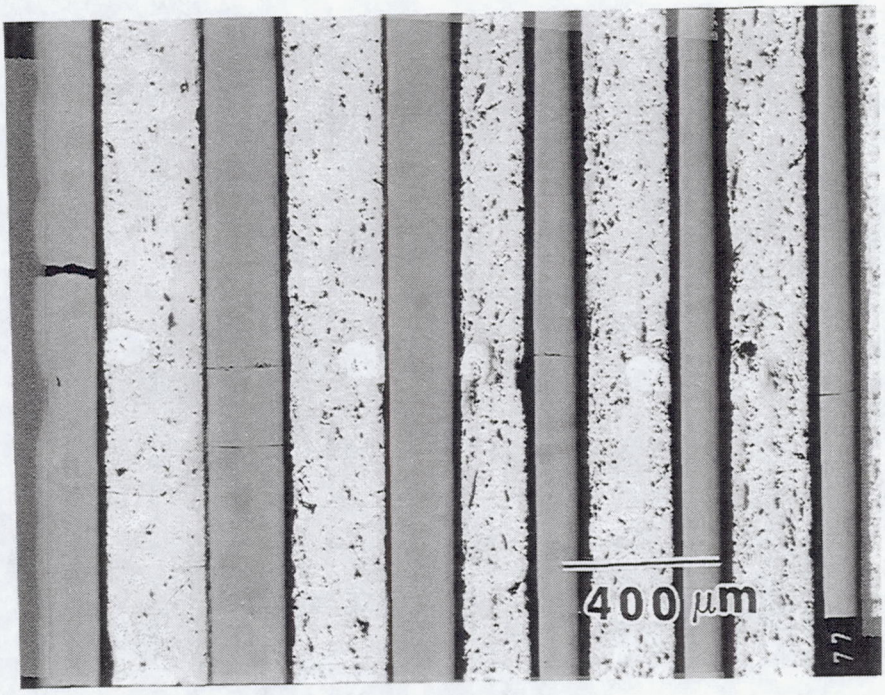

Figure 34. Distributed fiber cracks confined to Mo-ribbon sites in specimen F41-14 (300 cycles at 300 MPa).

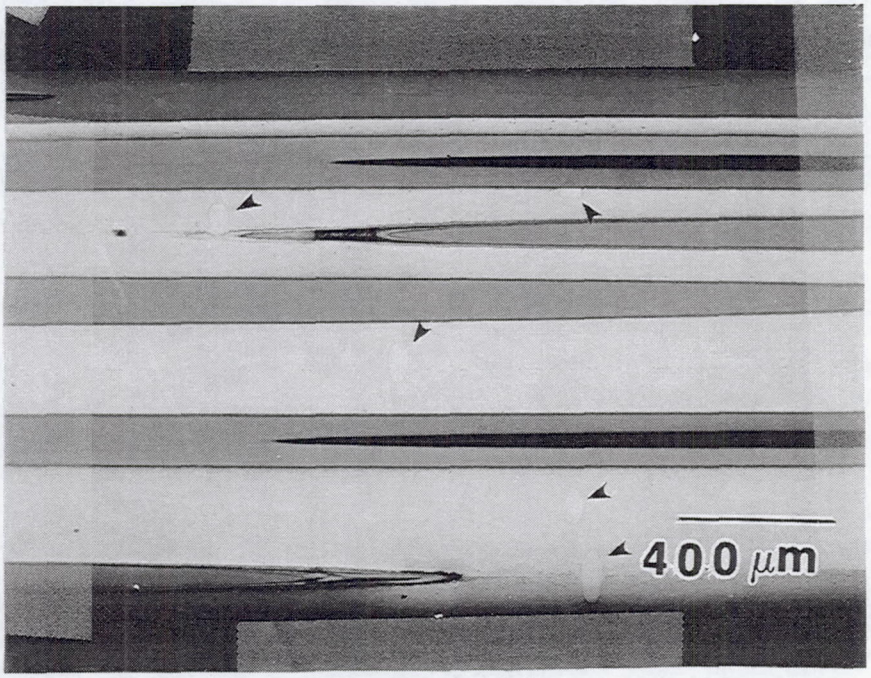

Figure 35. Dispersed Mo-ribbons in MMC specimen as viewed from edge of specimen near gage section.

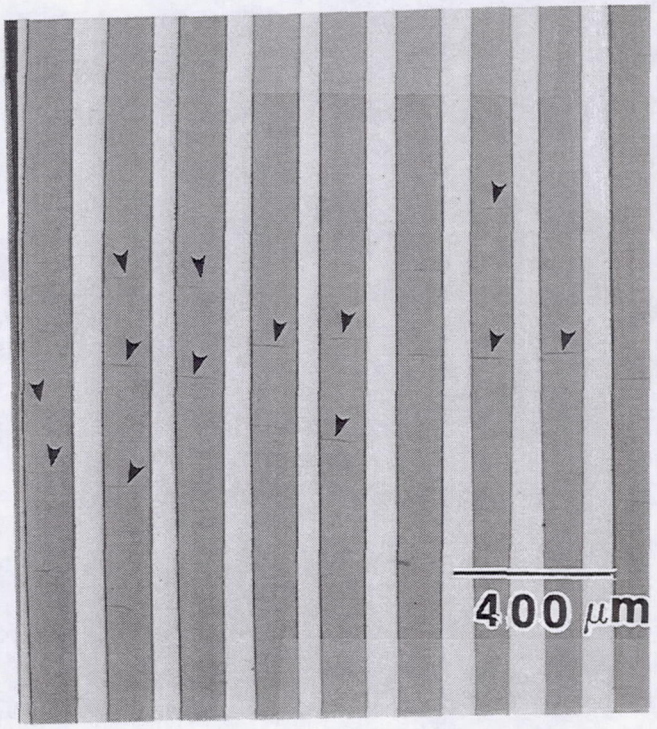

Figure 36. Distributed fiber cracking in a specimen (30 vol % MMC) without Mo weaves which was cycled at 512 MPa max. stress with 2 min cycle time (300-538 C) in IP TMF.

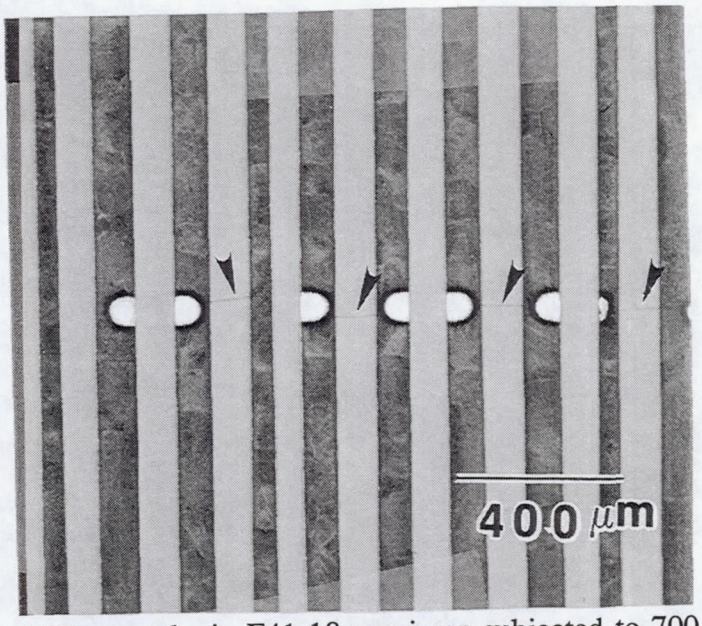

Figure 37. Distributed fiber cracks in F41-18 specimen subjected to 700 MPa max. stress for 200 cycles with 16 min cycle time (300-538 C).

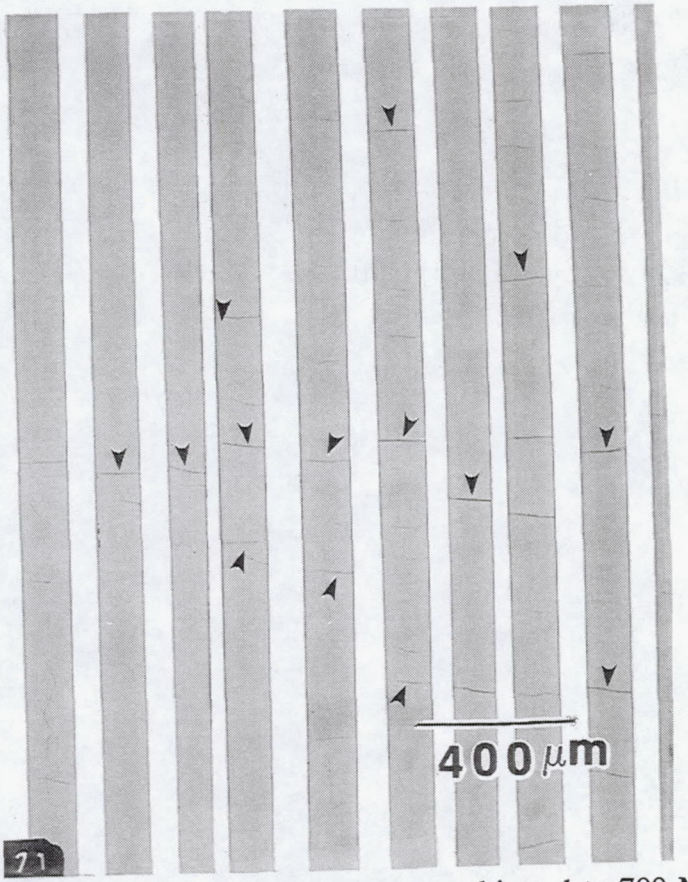

Figure 38. Distributed fiber cracks in F41-21 specimen subjected to 700 MPa max. stress for 200 cycles with 2 min cycle time (300-538 C).

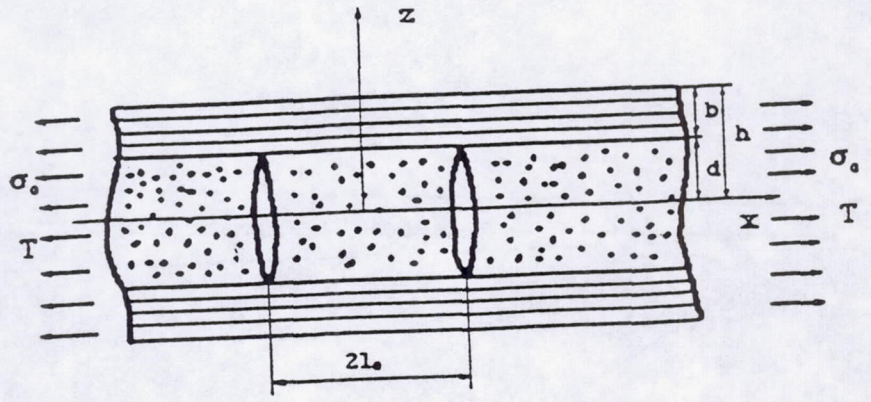

Figure 39. Schematic showing the geometry of an element of a $[0_m 90_n]_s$ cross-poly laminate subjected to an uniaxial remote stress and temperature.

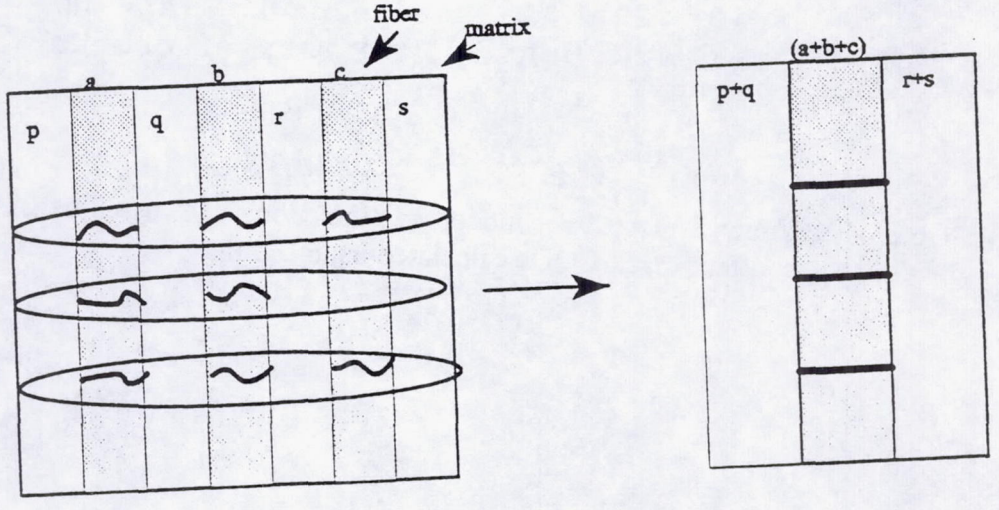

Figure 40. Multiple fiber cracks and nonconservative equivalent crack analogy.

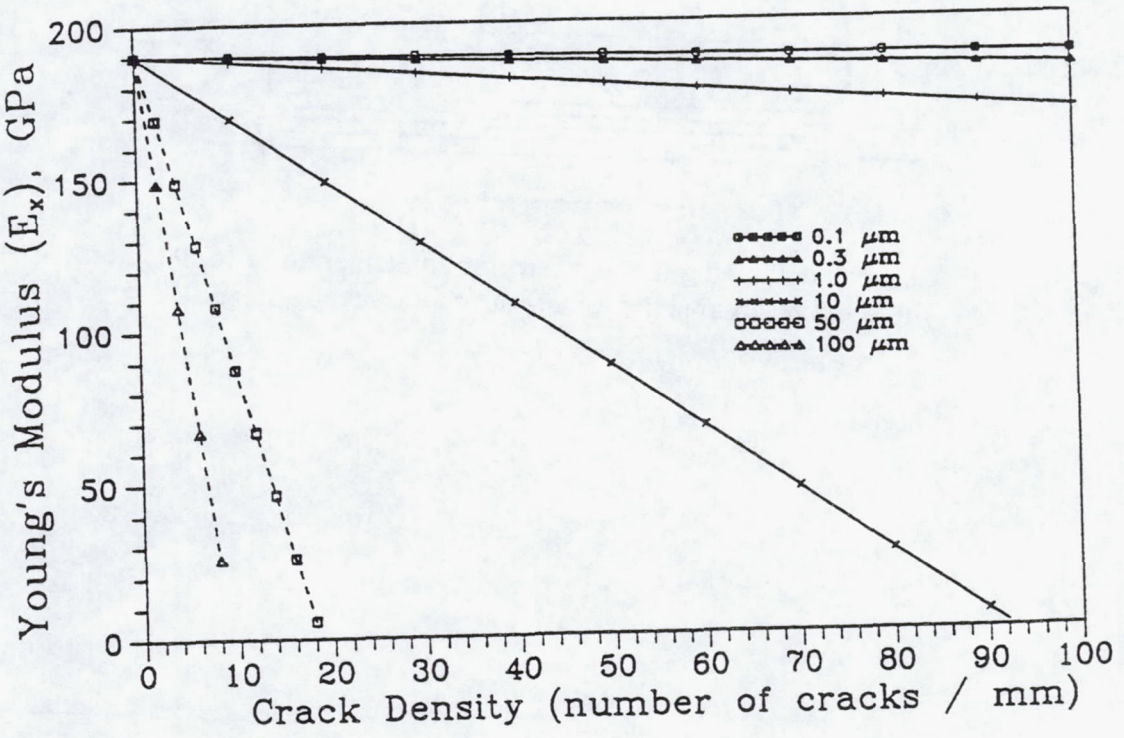

Figure 41. Young's modulus reduction as a function of the crack density for various constant crack CODs calculated using Eqn. 1.

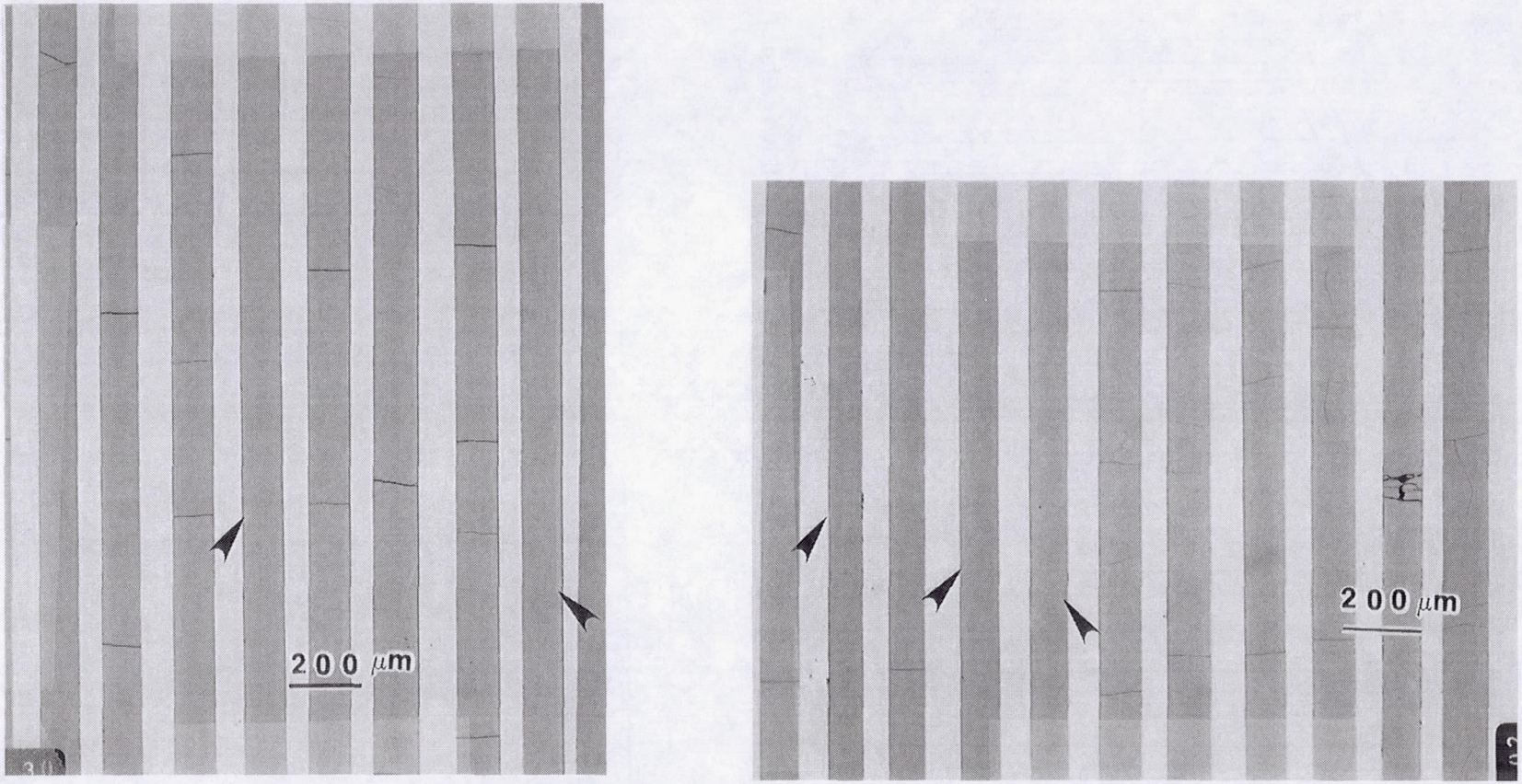

(a) (b)

Figure 42 a,b. Long load carrying unbroken ligaments (shown by arrows) in a IP TMF specimen (41-1, N_f = 94.5 cycles) with distributed fiber cracks.

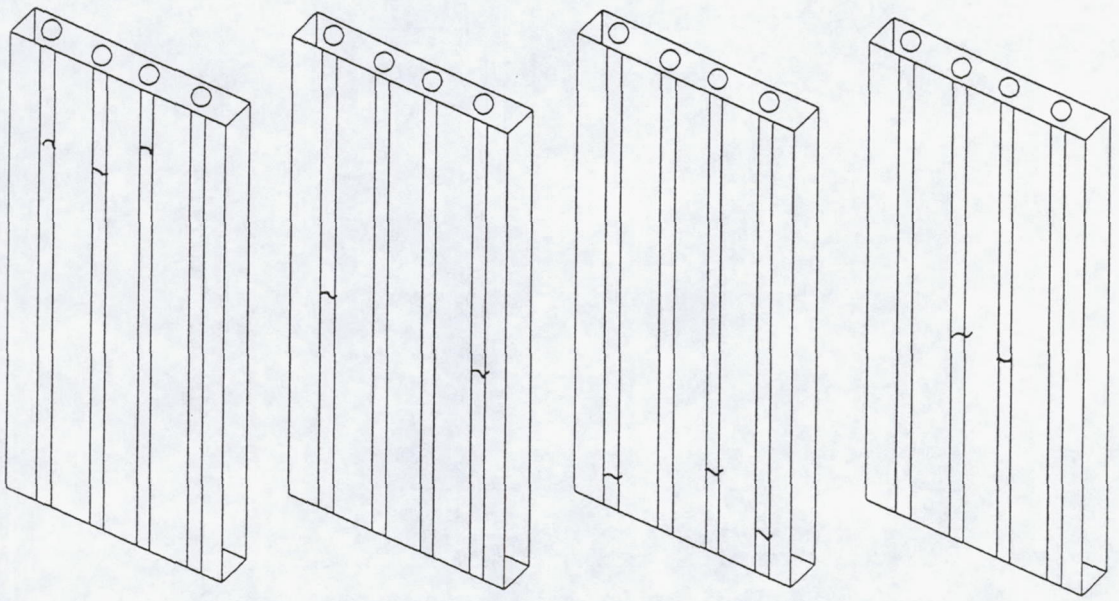

Figure 43. Nonplanar fiber cracks in each ply which may not lead to specimen failure.

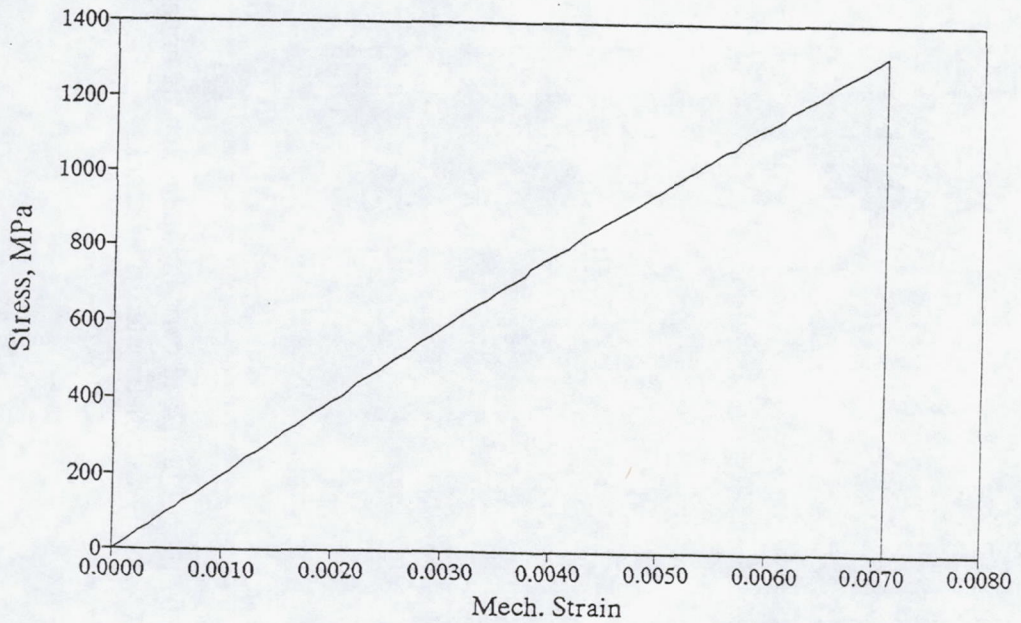

Figure 44. Stress-strain curve (residual strength 1314 MPa) for a MMC specimen (F41-23) cycled at 850 MPa max. stress for 300 IP TMF cycles.

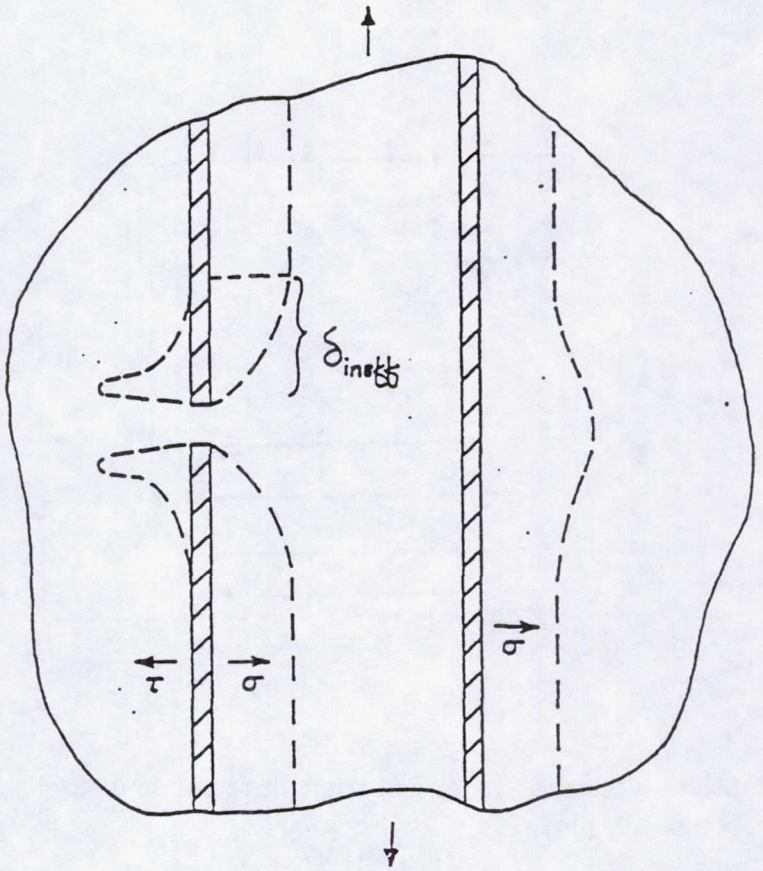

Figure 45. Stress intensification in a neighboring fiber as influenced by ineffective length of cracked fiber [30].

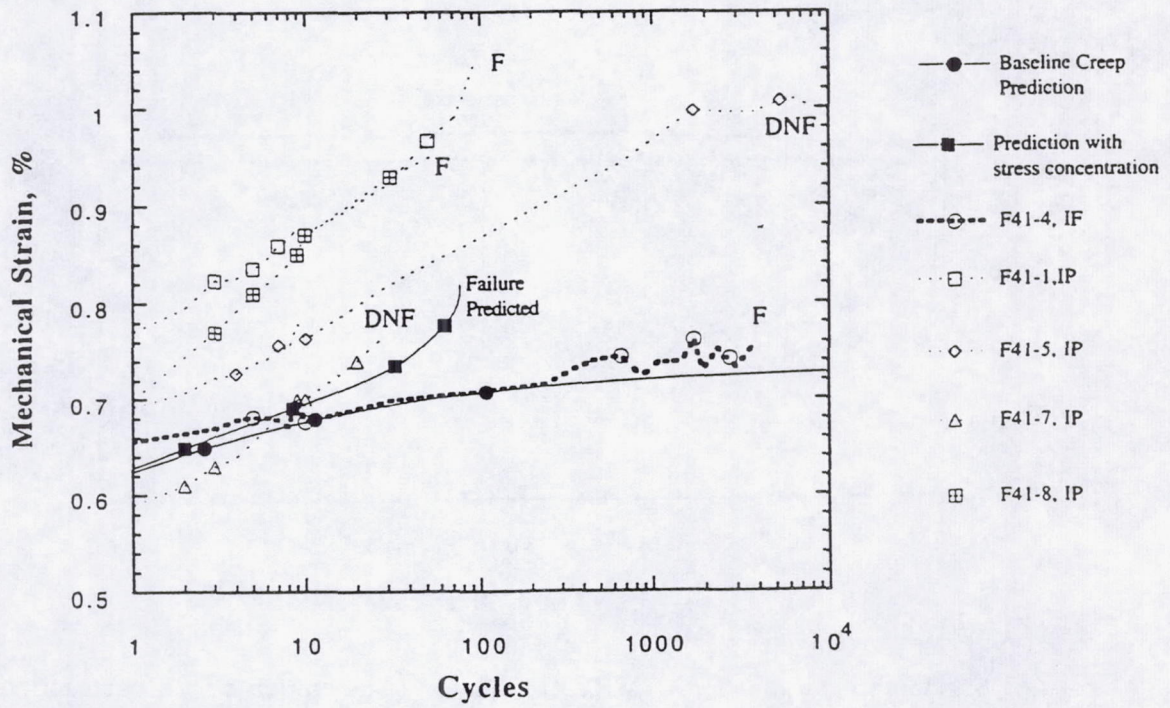

Figure 46. Comparison of experimental ratchetting curves (dashed lines) at 1114 MPa for IP and IF specimens, with the predictions of the modified creep model (solid lines) that accounts for fiber fracture. Infinite life is predicted for baseline conditions (bottom solid line), whereas a life below 80 cycles is predicted if a stress concentration of 1.25 is introduced (upper solid line).

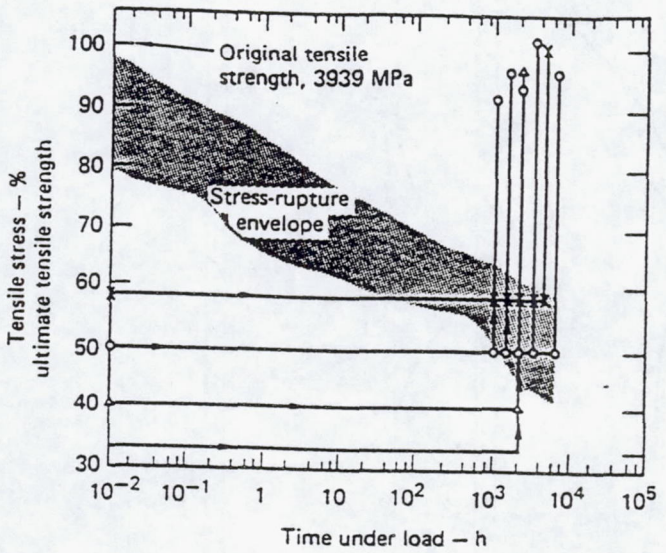

Figure 47. Stress-rupture behavior and strength retention of S-glass/epoxy unidirectional composite [34].

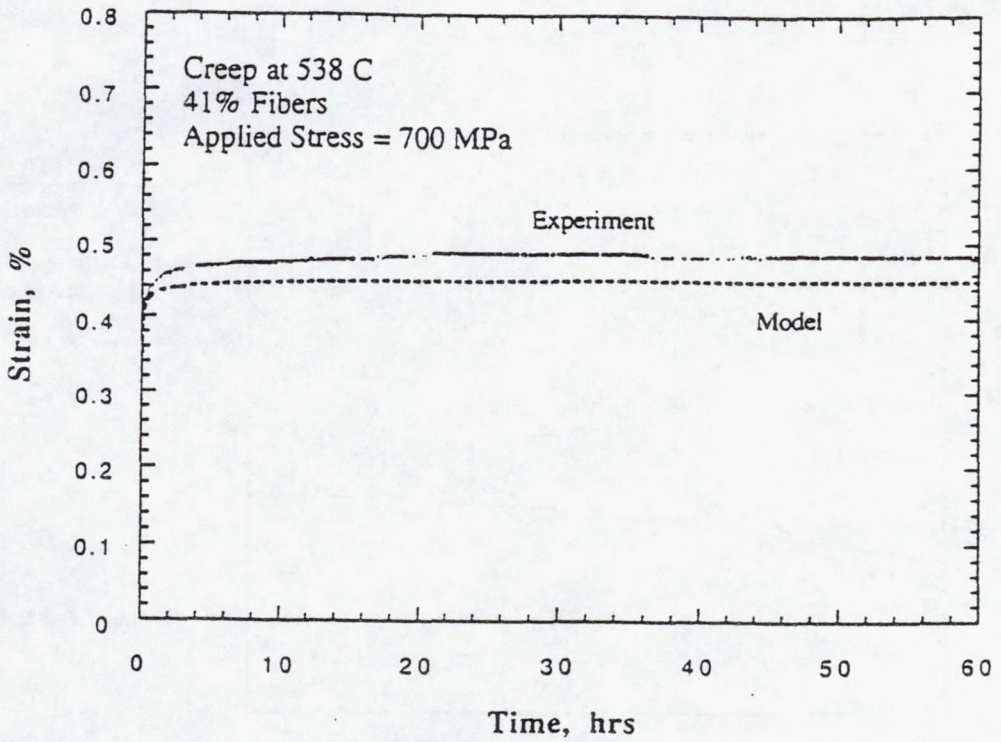

Figure 48. Creep curve at 700 MPa at 538 C. The upper curve corresponds to experimental data, and the lower curve is the theoretical prediction based on isostrain conditions and secondary creep for the matrix.

REPORT DOCUMENTATION PAGE

Form Approved
OMB No. 0704-0188

1. AGENCY USE ONLY (*Leave blank*)	2. REPORT DATE	3. REPORT TYPE AND DATES COVERED
	June 1995	Final Contractor Report

4. TITLE AND SUBTITLE

In-Phase Thermomechanical Fatigue Mechanisms in an Unidirectional SCS-6/Ti 15-3 MMC

5. FUNDING NUMBERS

WU–505–63–12
C–NAS3–26822

6. AUTHOR(S)

Golam M. Newaz and Bhaskar S. Majumdar

7. PERFORMING ORGANIZATION NAME(S) AND ADDRESS(ES)

Battelle Memorial Institute
505 King Avenue
Columbus, Ohio 43201

8. PERFORMING ORGANIZATION REPORT NUMBER

E–9716

9. SPONSORING/MONITORING AGENCY NAME(S) AND ADDRESS(ES)

National Aeronautics and Space Administration
Lewis Research Center
Cleveland, Ohio 44135–3191

10. SPONSORING/MONITORING AGENCY REPORT NUMBER

NASA CR–195482

11. SUPPLEMENTARY NOTES

Golam M. Newaz, Battelle Memorial Institute, 505 King Avenue, Columbus, Ohio 43201 (work funded by NASA Contract NAS3–26822), and Bhaskar S. Majumdar, Universal Energy Systems, 4401 Dayton-Xenia Rd., Dayton, Ohio 45432. Project Manager, Brad Lerch, Structures Division, NASA Lewis Research Center, organization code 5220, (216) 433–5522.

12a. DISTRIBUTION/AVAILABILITY STATEMENT

Unclassified - Unlimited
Subject Category 24

This publication is available from the NASA Center for Aerospace Information, (301) 621–0390.

12b. DISTRIBUTION CODE

13. ABSTRACT ***(Maximum 200 words)***

The objective of this investigation was to identify the inelastic deformation and damage mechanisms under in-phase (IP) thermomechanical fatigue (TMF) in a unidirectional SCS-6/Ti 15-3 metal matrix composite (MMC). Load-controlled IP TMF tests were conducted at 300-538 °C at various stress ranges in high-purity argon. A major emphasis of this work was to identify damage mechanism well before final fracture of specimens, rather than to generate life diagrams, to aid development of a realistic deformation/damage and life model.

14. SUBJECT TERMS

Metal matrix composite; Fatigue; SiC/Ti-15-3; Deformation; Damage

15. NUMBER OF PAGES

67

16. PRICE CODE

A04

17. SECURITY CLASSIFICATION OF REPORT	18. SECURITY CLASSIFICATION OF THIS PAGE	19. SECURITY CLASSIFICATION OF ABSTRACT	20. LIMITATION OF ABSTRACT
Unclassified	Unclassified	Unclassified	